Direct Estimation of Information Shares in Higher-Order Continuous-Time Models – Online Appendix

Karsten Schweikert* Daniel González Olivares
University of Hohenheim Universidad de Guadalajara
Gustavo Fruet Dias
University of East Anglia & CREATES

[Latest update: September 14, 2026]

A Proofs

Proof of Lemma 1. See the proof of Theorem 1 in Chambers (1999).

□

Lemma 2 (Supplementary model).

The exact discrete-time model under our observed vector x_t, that holds for $t = 1, \ldots, k$, evolves according to the discrete-time vector error correction model representation

$$\begin{aligned} x_h &= G_1 y(0) + \eta_h, \\ \Delta x_{th} &= \Lambda_t(\theta) x_{th-h} + \Upsilon_1(\theta)\Delta x_{th-h} + \Upsilon_2(\theta)\Delta x_{th-2h} + \cdots \\ &\quad + \Upsilon_{t-2}(\theta)\Delta x_{2/h} + G_t y(0) + \eta_{th}, \qquad t = 2, \ldots, k, \end{aligned} \tag{A.1}$$

where

$$\Lambda_t = J_1 + \cdots + J_{t-1} - I, \qquad \Upsilon_l = -\sum_{j=l+1}^{t-1} J_j, \quad l = 1, \ldots, t-2, \; t = 3, \ldots, k,$$

$$\eta_h = S_1 \int_0^h e^{(1-s)A} \zeta^*(ds), \qquad \eta_{2h} = \varepsilon_{1,2h} + C_{12} S_2 \int_0^h e^{(1-s)A} \zeta^*(ds),$$

$$J_1 = C_{11}, \qquad J_t = C_{12} \sum_{j=1}^{t-1} C_{22}^{j-1} C_{21}, \quad t = 2, \ldots, k-1,$$

*Address: University of Hohenheim, Core Facility Hohenheim & Institute of Economics, Schloss Hohenheim 1 C, 70593 Stuttgart, Germany, e-mail: *karsten.schweikert@uni-hohenheim.de*

$$G_1 = S_1 e^A, \qquad\qquad G_t = C_{12} C_{22}^{t-2} S_2 e^A \quad t = 2, \ldots, k,$$

$$\eta_{th} = \varepsilon_{1,th} + C_{12} \sum_{j=0}^{t-3} C_{22}^{j} \varepsilon_{2,th-h-jh} + C_{12} C_{22}^{t-2} S_2 \int_0^h e^{(1-s)A} \zeta^*(ds), \qquad t = 3, \ldots, k.$$

Proof of Lemma 2. See the proof of Theorem 2 in Chambers (1999).

□

Lemma 3 (Moving average representation of η_{th})**.**

The moving average representation of the discrete-time disturbance vectors is given by

$$\begin{aligned} \eta_{th} &= \sum_{i=0}^{j-1} P_i \varepsilon_{th-ih}, \qquad j = 1, \ldots, k, \\ \eta_{th} &= \sum_{i=0}^{k-1} R_i \varepsilon_{th-ih}, \quad t = (k+1), \ldots, T, \end{aligned} \tag{A.2}$$

where

$$\begin{aligned} P_0 &= S_1, \quad P_i = C_{12} C_{22}^{i-1} S_2, && i = 1, \ldots, k-1, \\ R_0 &= S_1, \quad R_i = C_{12}(M_{1i} S_1 + M_{i+1} S_2), && i = 1, \ldots, k-1, \\ M &= [M_1 \quad M_2 \quad \cdots \quad M_k], \\ M_1 &= [M_{11} \quad M_{12} \quad \cdots \quad M_{1,k-1}]. \end{aligned}$$

Also, if we define the $nT \times 1$ vector $\eta = [(\eta_h)', (\eta_{2h})', \cdots, (\eta_{Th})']'$, then, its autocovariance representation is given by

$$\Omega = E[\eta \eta'], \tag{A.3}$$

where

$$\begin{aligned} E[\eta_{th}(\eta_{th-jh})'] &= \Omega_{t,t-j} = \sum_{i=j}^{t-1} P_i \Omega_\varepsilon (P_{i-j})', && t = 1, \ldots, k, && j = 0, \ldots, t-1, \\ E[\eta_{th}(\eta_{th-jh})'] &= \Omega_{t,t-j} = \sum_{i=j}^{k-1} R_i \Omega_\varepsilon (P_{i-j})', && t = k+1, \ldots, 2k-1, && j = t-k, \ldots, k-1, \\ E[\eta_{th}(\eta_{th-jh})'] &= \Omega_j = \sum_{i=j}^{k-1} R_i \Omega_\varepsilon (R_{i-j})', && t = k+1+j, \ldots, T, && j = 0, \ldots, k-1, \\ E[\eta_{th}(\eta_{th-jh})'] &= 0, && t = k+2, \ldots, T, && j > k-1, \end{aligned}$$

and

$$\Omega_\varepsilon = E[\varepsilon_{th}\varepsilon_{th}'] = \int_0^h e^{As}\Sigma^* e^{A's} ds,$$

with $\Sigma^* = C^*(C^*)'$.

Proof of Lemma 3. See the proof of Theorem 3 in Chambers (1999).

□

Proof of Theorem 1. The first part of the proof closely follows the proof of Proposition 7 in Comte (1999). Multiplying the EC form in (4) by α and $\alpha_\perp$, respectively and noting that $A_0 = \alpha\beta'$ and $\alpha_\perp'\alpha = 0_{(n-r)\times r}$ gives

$$\begin{aligned} -\alpha'\alpha\beta' x(t) + \alpha'\phi(D)Dx(t) &= \alpha' u(dt) && \text{(A.4)} \\ \alpha_\perp'\phi(D)Dx(t) &= \alpha_\perp' u(dt). && \text{(A.5)} \end{aligned}$$

Since the system is not invertible in x and Dx, we define new variables

$$Z(t) = (\beta'\beta)^{-1}\beta' x(t), \qquad V(t) = (\beta_\perp'\beta_\perp)^{-1}\beta_\perp' Dx(t). \tag{A.6}$$

If we further define $\bar{\beta} = \beta(\beta'\beta)^{-1}$ and $\bar{\beta}_\perp = \beta_\perp(\beta_\perp'\beta_\perp)^{-1}$, then the full rank $n \times n$ matrix $R = (\beta, \beta_\perp)$ satisfies $R(R'R)^{-1}R' = I_n$ so that $\beta\bar{\beta}' + \beta_\perp\bar{\beta}_\perp' = I_n$. This implies that

$$Dx(t) = (\beta\bar{\beta}' + \beta_\perp\bar{\beta}_\perp')Dx(t) = \beta DZ(t) + \beta_\perp V(t). \tag{A.7}$$

Substituting in and noting that $\beta' x(t) = \beta'\beta Z(t)$, we have

$$\begin{aligned} -\alpha'\alpha(\beta'\beta)Z(t) + \alpha'\phi(D)\beta DZ(t) + \alpha'\phi(D)\beta_\perp V(t) &= \alpha' u(dt) && \text{(A.8)} \\ \alpha_\perp'\phi(D)\beta DZ(t) + \alpha_\perp'\phi(D)\beta_\perp V(t) &= \alpha_\perp' u(dt). && \text{(A.9)} \end{aligned}$$

Then, we can express the system using a lag polynomial so that $\tilde{P}(D)(Z(t)', V(t)')' = (\alpha, \alpha_\perp)' u(dt)$ with

$$\tilde{P}(D) = \begin{pmatrix} -\alpha'\alpha(\beta'\beta) + \alpha'\phi(D)\beta D & \alpha'\phi(D)\beta_\perp \\ \alpha_\perp'\phi(D)\beta D & \alpha_\perp'\phi(D)\beta_\perp \end{pmatrix}. \tag{A.10}$$

It can easily be verified that $\det(\tilde{P}(0)) = (-1)^r \det(\alpha'\alpha)\det(\beta'\beta)\det(\alpha_\perp'\phi(0)\beta_\perp)$ which is nonzero due to Assumptions 4 and 5. For $z \neq 0$, we can write $\tilde{P}(z) = (\alpha, \alpha_\perp)' P(z)(\beta, \beta_\perp/z)$ so that

$$\det(\tilde{P}(z)) = \frac{1}{z^{n-r}} \det((\alpha, \alpha_\perp)')\det(P(z))\det((\beta, \beta_\perp)). \tag{A.11}$$

We conclude that $\tilde{P}(z)$ has the same roots as $P(z)$ except for the null ones, and the nonzero roots of P are stable due to Assumption 3. Thus, the transformed system in (Z, V) is stable and admits a unique causal second-order stationary solution. Now with null initial conditions, we have

$$\begin{pmatrix} Z(t) \\ V(t) \end{pmatrix} = \int_{-\infty}^{t} [\exp(\bar{\tilde{A}}(t-s))]_{1,k}(\alpha, \alpha_\perp)' u(ds), \tag{A.12}$$

where $\bar{\tilde{A}}$ is the companion matrix matching the lag polynomial $\tilde{P}(z)$ and the integral is understood in the mean-square sense. The corresponding impulse-response matrix for $x(t)$ is denoted by $A(x)$. Its first r rows are determined by the stationary response $f(x)$, while the remaining rows are obtained by integrating $f(x)$. Thus,

$$A(x) = (\beta, \beta_\perp) \begin{pmatrix} f_{1,1}(x) & \cdots & f_{1,n}(x) \\ \vdots & & \vdots \\ f_{r,1}(x) & \cdots & f_{r,n}(x) \\ F_{r+1,1}(x) & \cdots & F_{r+1,n}(x) \\ \vdots & & \vdots \\ F_{n,1}(x) & \cdots & F_{n,n}(x) \end{pmatrix}' (\alpha, \alpha_\perp), \tag{A.13}$$

where $F_{i,j}(x) = \int_0^x f_{i,j}(s)\, ds$. Since $\widetilde{A}$ is stable, it holds that $\lim_{x\to\infty} f_{i,j}(x) = 0$. Moreover,

$$\int_0^\infty f(s)\, ds = -\left[\widetilde{A}^{-1}\right]_{1,k} = -\widetilde{P}(0)^{-1}, \tag{A.14}$$

using the inverse companion-matrix formula under the sign convention adopted above. Consequently, we have

$$A(\infty) = -\beta_\perp \left(\alpha'_\perp \phi(0) \beta_\perp\right)^{-1} \alpha'_\perp = \beta_\perp \left(\alpha'_\perp A_1 \beta_\perp\right)^{-1} \alpha'_\perp, \tag{A.15}$$

because $\phi(0) = -A_1$. Since $\alpha'_\perp A_1 \beta_\perp$ is nonsingular and $\alpha_\perp$ and $\beta_\perp$ have rank $n-r$, it follows that $\operatorname{rank}(A(\infty)) = n - r$, $\beta' A(\infty) = 0$, and $A(\infty)\alpha = 0$.

Define $\widetilde{A}(x) := A(x) - A(\infty)$. The stable part of the impulse response decays exponentially, so

$$\int_0^\infty \|\widetilde{A}(x)\|^2\, dx < \infty. \tag{A.16}$$

Since $u(ds)$ is defined on the whole real line, the process

$$x^{\mathrm{st}}(t) := \int_{-\infty}^{t} \widetilde{A}(t-s) u(ds) \tag{A.17}$$

is well-defined in the mean-square sense and is second-order stationary.

Now define $U(t) := u((0,t])$ and the permanent component $M(t) := A(\infty)U(t)$. For $0 \leq s \leq t$, it holds that

$$M(t) - M(s) = A(\infty)u((s,t]). \tag{A.18}$$

Assumption 1 states that $E\big(u((s,t]) \mid \mathcal{F}_s\big) = 0$. Therefore,

$$E\big(M(t) - M(s) \mid \mathcal{F}_s\big) = A(\infty)E\big(u((s,t]) \mid \mathcal{F}_s\big) = 0. \tag{A.19}$$

Thus, $E\big(M(t) \mid \mathcal{F}_s\big) = M(s)$, and $M(t)$ is a square-integrable martingale.

Finally, the solution for null initial conditions can be written as

$$\begin{aligned} x(t) &= M(t) + x^{\mathrm{st}}(t) && \text{(A.20)} \\ &= A(\infty)U(t) + \int_{-\infty}^{t} \widetilde{A}(t-s)u(ds). && \text{(A.21)} \end{aligned}$$

$\square$

Proof of Theorem 2. By Lemma 1, the sampled process x_{th} admits as its exact discrete-time representation a finite-dimensional Gaussian VAR in error-correction form. Under Assumptions 3–5, this representation is an $I(1)$ cointegrated system with cointegration rank r, while Assumption 6 guarantees that Π, $\Gamma_1, \ldots, \Gamma_{k-1}$, and η_{th} are well defined. By Assumption 2, the innovations are Gaussian. The defined parameter space is $\theta \in \Theta$ and the sample is denoted by $\boldsymbol{x}$. $\log L(\boldsymbol{x}, \theta)$ is a measurable function of $\boldsymbol{x}$ for all $\theta \in \Theta$ and $\partial \log L/\partial\theta$ exists and is continuous in an open neighborhood of θ_0. Further, $\log L(\theta)$ attains a strict local maximum at θ_0. Under Assumption 8, $\partial^2 \log L/\partial\theta\partial\theta'$ exists and is continuous in an open convex neighborhood of θ_0. Hence the Gaussian likelihood associated with the exact discrete-time representation satisfies the standard regularity conditions for maximum likelihood estimation in correctly specified cointegrated Gaussian VAR models; see Theorem 4.1.3 in Amemiya (1985) and Theorem 3.3 in Newey and McFadden (1994). In particular, it holds that $\hat{\theta} \xrightarrow{p} \theta_0$.

Since $\hat{\theta}$ is an interior maximizer of the log-likelihood,

$$\left.\frac{\partial \log L}{\partial\theta}\right|_{\hat{\theta}} = 0. \tag{A.22}$$

A mean-value expansion around θ_0 yields

$$\left.\frac{\partial \log L}{\partial\theta}\right|_{\hat{\theta}} = \left.\frac{\partial \log L}{\partial\theta}\right|_{\theta_0} + \left.\frac{\partial^2 \log L}{\partial\theta\partial\theta'}\right|_{\theta^*} (\hat{\theta} - \theta_0), \tag{A.23}$$

where θ^* lies between $\hat{\theta}$ and θ_0. Rearranging gives

$$\sqrt{T}(\hat{\theta}-\theta_0) = -\left[\frac{1}{T}\left.\frac{\partial^2 \log L}{\partial\theta\partial\theta'}\right|_{\theta^*}\right]^{-1}\frac{1}{\sqrt{T}}\left.\frac{\partial \log L}{\partial\theta}\right|_{\theta_0}. \tag{A.24}$$

Again by Theorem 4.1.3 in Amemiya (1985) and Theorem 3.3 in Newey and McFadden (1994), applied to the correctly specified Gaussian likelihood,

$$\frac{1}{\sqrt{T}}\left.\frac{\partial \log L}{\partial\theta}\right|_{\theta_0} \xrightarrow{d} \mathcal{N}(0, B(\theta_0)), \tag{A.25}$$

where

$$B(\theta_0) = \lim_{T\to\infty} E\left[\frac{1}{T}\frac{\partial \log L}{\partial\theta}\bigg|\,\theta_0\,\left.\frac{\partial \log L}{\partial\theta'}\right|_{\theta_0}\right], \tag{A.26}$$

and, since $\hat{\theta} \xrightarrow{p} \theta_0$, also $\theta^* \xrightarrow{p} \theta_0$, so that

$$\frac{1}{T}\left.\frac{\partial^2 \log L}{\partial\theta\partial\theta'}\right|_{\theta^*} \xrightarrow{p} A(\theta_0), \tag{A.27}$$

with

$$A(\theta_0) = \lim_{T\to\infty} E\left[\frac{1}{T}\left.\frac{\partial^2 \log L}{\partial\theta\partial\theta'}\right|_{\theta_0}\right]. \tag{A.28}$$

Therefore, by Slutsky's theorem,

$$\sqrt{T}(\hat{\theta}-\theta_0) \xrightarrow{d} \mathcal{N}\Big(0, A(\theta_0)^{-1}(\theta_0)A(\theta_0)^{-1}\Big). \tag{A.29}$$

Finally, under correct Gaussian specification, the information matrix equality implies $B(\theta_0) = -A(\theta_0)$. Hence, defining

$$\Sigma_{\theta_0} = -\lim_{T\to\infty} E\left[\frac{1}{T}\left.\frac{\partial^2 \log L}{\partial\theta\partial\theta'}\right|_{\theta_0}\right], \tag{A.30}$$

we obtain

$$\sqrt{T}(\hat{\theta}-\theta_0) \xrightarrow{d} \mathcal{N}(0, \Sigma_{\theta_0}^{-1}), \tag{A.31}$$

which proves the theorem.

□

Proof of Corollary 1. Since β is known, we can directly compute a suitable orthogonal complement $\beta_\perp$. We now turn to the parameters estimated by maximizing the log-likelihood derived from the exact discrete-time representation. Without loss of generality, we choose

$\hat{\alpha}_\perp = \alpha_\perp - \alpha(\hat{\alpha}'\alpha)^{-1}\hat{\alpha}'\alpha_\perp$, then $\hat{\alpha}'\hat{\alpha}_\perp = 0$ and

$$\hat{\alpha}_\perp - \alpha_\perp = -\hat{\bar{\alpha}}(\hat{\alpha} - \alpha)'\alpha_\perp, \tag{A.32}$$

where $\hat{\bar{\alpha}} = \alpha(\hat{\alpha}'\alpha)^{-1}$. Using the property $\hat{\alpha} \xrightarrow{p} \alpha$ which follows from Theorem 2 and the CMT, we have $\hat{\bar{\alpha}} \xrightarrow{p} \bar{\alpha} = \alpha(\alpha'\alpha)^{-1}$ and finally $\hat{\alpha}_\perp \xrightarrow{p} \alpha_\perp$.

Furthermore, it follows from Theorem 2 that $\hat{A}_1 \xrightarrow{p} A_1$ and $\hat{\Sigma} = \hat{C}\hat{C}' \xrightarrow{p} CC' = \Sigma$. Since Assumption 5 implies that $\alpha_\perp' A_1 \beta_\perp$ is nonsingular, the CMT yields

$$\hat{A}(\infty) = \beta_\perp(\hat{\alpha}_\perp'\hat{A}_1\beta_\perp)^{-1}\hat{\alpha}_\perp' \xrightarrow{p} \beta_\perp(\alpha_\perp' A_1\beta_\perp)^{-1}\alpha_\perp' = A(\infty). \tag{A.33}$$

Choosing a common row $\hat{\xi}$ of $\hat{A}(\infty)$ and a fixed informational ordering of the markets to identify C, it follows that

$$\frac{[\hat{\xi}\hat{C}]_j^2}{\hat{\xi}\hat{\Sigma}\hat{\xi}} \xrightarrow{p} \frac{[\xi C]_j^2}{\xi\Sigma\xi}, \tag{A.34}$$

which concludes the proof.

□

Proof of Theorem 3. Theorem 2 implies that any subset of the ML estimator is normally distributed. Hence, $\gamma = \text{vec}(\alpha, A_1)$ is also normally distributed

$$\sqrt{T}(\hat{\gamma} - \gamma) \xrightarrow{d} \mathcal{N}(0, \Sigma_\gamma^{-1}), \tag{A.35}$$

with covariance matrix Σ_γ^{-1} that can be obtained as a conformable partition of the covariance matrix $\Sigma_{\theta_0}^{-1}$. Now, we turn to the matrix $A_\infty = A(\infty) = \beta_\perp(\alpha_\perp' A_1\beta_\perp)^{-1}\alpha_\perp'$ that depends only on α and A_1 (and the known cointegration matrix β). Applying the delta method, we have

$$\sqrt{T}(\text{vec}(\hat{A}_\infty) - \text{vec}(A_\infty)) \xrightarrow{d} \mathcal{N}(0, \Sigma_{A_\infty}^{-1}), \tag{A.36}$$

with

$$\Sigma_{A_\infty}^{-1} = \frac{\partial\,\text{vec}(A_\infty)}{\partial\gamma'}\Sigma_\gamma^{-1}\frac{\partial\,\text{vec}(A_\infty')}{\partial\gamma}. \tag{A.37}$$

From Vlaar (2004), we know that

$$\frac{\partial\,\text{vec}(A_\infty)}{\partial\gamma'} = \Big(\left(A_\infty' A_1' - I_n\right) H_{\alpha_1'}(\alpha' H_{\alpha_1'})^{-1}, A_\infty'\Big) \otimes A_\infty', \tag{A.38}$$

where $H_{\alpha_1'}$ is a 0-1 selection matrix so that $(\alpha' H_{\alpha_1'})$ is non-singular. $H_{\alpha_2'}$ selects the remaining columns and allows for the expression of the orthogonal complement as

$$\alpha_\perp = H_{\alpha_2'} - H_{\alpha_1'}(\alpha' H_{\alpha_1'})^{-1}\alpha' H_{\alpha_2'}. \tag{A.39}$$

Without loss of generality, we select the first of the common rows and denote the row with ξ. We define the selection matrix P that extracts the needed components of A_∞ so that $\hat{\xi} = PA_\infty$ and have the following convergence in distribution

$$\sqrt{T}\,(\widehat{\xi} - \xi) \xrightarrow{d} \mathcal{N}(0, P\Sigma_{A_\infty}^{-1}P'). \tag{A.40}$$

We denote the covariance matrix by $\Sigma_\xi = P\Sigma_{A_\infty}^{-1}P'$.

Because the Cholesky factor C is estimated directly, we know that

$$\sqrt{T}\,\mathrm{vec}(\widehat{C} - C) \ \xrightarrow{d}\ \mathcal{N}(0, \Sigma_C), \tag{A.41}$$

where Σ_C is also a conformable partition of $\Sigma_{\theta_0}^{-1}$.

Now, we need to consider the joint convergence of $(\hat{\xi}', \hat{C}')'$. By ordinary algebra, we have

$$\widehat{\xi}\,\widehat{C} - \xi\,C = (\widehat{\xi} - \xi)\,C + \xi\,(\widehat{C} - C) + (\widehat{\xi} - \xi)\,(\widehat{C} - C).$$

Since both $\widehat{\xi} - \xi$ and $\widehat{C} - C$ are $O_p(T^{-1/2})$, the last term is $o_p(T^{-1/2})$. Hence,

$$\sqrt{T}\,(\widehat{\xi}\,\widehat{C} - \xi\,C) = C\,\sqrt{T}\,(\widehat{\xi} - \xi)\ +\ \xi\,\sqrt{T}\,(\widehat{C} - C) + o_p(1).$$

For the derivation of the asymptotic covariance matrix, we need to vectorize the second term:

$$\sqrt{T}\,\mathrm{vec}(\widehat{\xi}\,\widehat{C} - \xi\,C) = C'\,\sqrt{T}\,(\widehat{\xi} - \xi)\ +\ (I_N \otimes \xi)\,\sqrt{T}\,\mathrm{vec}(\widehat{C} - C)\ +\ o_p(1).$$

We can apply the multivariate Delta method again and find for the inner product[1]

$$\sqrt{T}\,\mathrm{vec}(\widehat{\xi}\,\widehat{C} - \xi\,C) \ \xrightarrow{d}\ \mathcal{N}\Big(0,\ W\Big),$$

where

$$W = C'\,\Sigma_\xi\,C + (I_n \otimes \xi)\,\Sigma_C\,(I_n \otimes \xi)' + C'\,\Sigma_{\xi,C}\,(I_n \otimes \xi)' + (I_n \otimes \xi)\,\Sigma_{C,\xi}\,C.$$

Rearranging the terms yields $\hat{\xi}\hat{C} \overset{a}{\sim} N(\xi C, T^{-1}W)$. We denote the covariance matrix by $Z = T^{-1}W$.

At this point, we again apply the multivariate delta method. For this purpose, we first define $\hat{\vartheta} = \hat{\xi}\hat{C}$ and then rewrite $\hat{IS}_j^c$ so that

$$\hat{IS}_j^c = \frac{[\hat{\xi}\hat{C}]_j^2}{(\hat{\xi}\hat{C})(\hat{\xi}\hat{C})'} = \frac{\vartheta_j^2}{\sum_{i=1}^N \vartheta_i^2}, \qquad j = 1, \ldots, N. \tag{A.42}$$

[1]Under Gaussian (or symmetrically distributed) errors the cross-cumulant terms vanish, implying $\Sigma_{\xi,C} = \Sigma_{C,\xi}' = 0$.

Given that $\hat{\vartheta}$ is an n-dimensional vector with a normal distribution $\mathcal{N}(\vartheta, Z)$, the estimated information share is a continuous function of $\hat{\vartheta}$, i.e., $\hat{IS}_j^c = g_j(\hat{\vartheta}) = \hat{\vartheta}_j^2 / \sum_{i=1}^N \hat{\vartheta}_i^2$.

Now, we calculate the gradient $\nabla g_j(\hat{\vartheta})$. For convenience, let $s(\hat{\vartheta}) = \sum_{i=1}^N \hat{\vartheta}_i^2$. We can then write $g_j(\hat{\vartheta}) = \hat{\vartheta}_j^2 / s(\hat{\vartheta})$. Next, we need to find the partial derivatives of $g_j(\hat{\vartheta})$ with respect to each $\hat{\vartheta}_i$,

$$\frac{\partial g_j(\hat{\vartheta})}{\partial \hat{\vartheta}_i} = \frac{\partial}{\partial \hat{\vartheta}_i} \left(\frac{\hat{\vartheta}_j^2}{s(\hat{\vartheta})} \right), \tag{A.43}$$

and using the quotient rule yields

$$\frac{\partial}{\partial \hat{\vartheta}_i} \left(\frac{\hat{\vartheta}_j^2}{s(\hat{\vartheta})} \right) = \frac{s(\hat{\vartheta}) \frac{\partial \hat{\vartheta}_j^2}{\partial \hat{\vartheta}_i} - \hat{\vartheta}_j^2 \frac{\partial s(\hat{\vartheta})}{\partial \hat{\vartheta}_i}}{s(\hat{\vartheta})^2}. \tag{A.44}$$

For $i \neq j$, it holds that

$$\frac{\partial g_j(\hat{\vartheta})}{\partial \hat{\vartheta}_i} = -\frac{2\hat{\vartheta}_j^2 \hat{\vartheta}_i}{s(\hat{\vartheta})^2}, \tag{A.45}$$

and for $i = j$, we have

$$\frac{\partial g_j(\hat{\vartheta})}{\partial \hat{\vartheta}_j} = \frac{2\hat{\vartheta}_j \sum_{i \neq j} \hat{\vartheta}_i^2}{s(\hat{\vartheta})^2}. \tag{A.46}$$

Putting the partial derivatives together, we obtain the gradient vector,

$$\nabla g_j(\hat{\vartheta}) = \left(-\frac{2\hat{\vartheta}_j^2 \hat{\vartheta}_1}{s(\hat{\vartheta})^2}, -\frac{2\hat{\vartheta}_j^2 \hat{\vartheta}_2}{s(\hat{\vartheta})^2}, \dots, \frac{2\hat{\vartheta}_j \sum_{i \neq j} \hat{\vartheta}_i^2}{s(\hat{\vartheta})^2}, \dots, -\frac{2\hat{\vartheta}_j^2 \hat{\vartheta}_N}{s(\hat{\vartheta})^2} \right). \tag{A.47}$$

The delta method approximates $g_j(\hat{\vartheta}) \approx g_j(\vartheta) + (\nabla g_j(\vartheta))'(\hat{\vartheta} - \vartheta)$ where $\vartheta = \xi C$ is the mean vector. Given $\hat{\vartheta} \sim \mathcal{N}(\vartheta, Z)$, the distribution of $\hat{IS}_j^c$ using the delta method linear approximation is approximately normal with

$$\hat{IS}_j^c \overset{a}{\sim} \mathcal{N}\left(g_j(\vartheta), (\nabla g_j(\vartheta))' Z \nabla g_j(\vartheta)\right). \tag{A.48}$$

Standardizing the estimated information share then yields

$$\frac{\hat{IS}_j^c - IS_j^c}{\sqrt{(\nabla g_j(\vartheta))' Z \nabla g_j(\vartheta)}} = \frac{\sqrt{T}(\hat{IS}_j^c - IS_j^c)}{\sqrt{(\nabla g_j(\vartheta))' W \nabla g_j(\vartheta)}} \xrightarrow{d} \mathcal{N}(0, 1). \tag{A.49}$$

□

Theorem A.2. Under Assumptions 1 to 5 and 7, 8, the estimator $\hat{\theta}$ obtained by maximizing the Gaussian log-likelihood computed by the Kalman filter is consistent and asymptotically normally distributed,

$$\hat{\theta} \xrightarrow{p} \theta_0, \qquad \sqrt{T}(\hat{\theta} - \theta_0) \xrightarrow{d} \mathcal{N}(0, \Sigma_{\theta_0}^{-1}),$$

where

$$\Sigma_{\theta_0} = - \lim_{T\to\infty} E \frac{1}{T} \left. \frac{\partial^2 \log L_T(\theta)}{\partial\theta\partial\theta'} \right|_{\theta_0} .$$

Proof of Theorem A.2. The CAR(k) process admits the continuous-time state-space representation in (6). For observations at ticks t_τ, $\tau = 1, \ldots, T$, with durations $\delta_\tau = t_\tau - t_{\tau-1}$, the corresponding discrete-time state-space model is

$$x_\tau = Z_\tau y_\tau + v_\tau, \qquad y_\tau = e^{A(\theta)\delta_\tau} y_{\tau-1} + \varepsilon_\tau. \tag{A.50}$$

By Assumption 2, the state innovations are Gaussian. By construction, the measurement error v_τ is Gaussian as well. Hence the model is a linear Gaussian state-space system. Assumption 7(c) ensures that the covariance matrices of the state and measurement innovations are nonsingular, so the Gaussian prediction-error decomposition generated by the Kalman filter is well defined for all $\theta \in \Theta$.

Under Assumptions 3–5, the state vector contains an $I(1)$ component with cointegration rank r. Thus the model is a correctly specified nonstationary Gaussian state-space system. Assumption 7(b) guarantees that the durations remain bounded away from zero and infinity, so that the transition matrices $e^{A(\theta)\delta_\tau}$ and the corresponding innovation covariance matrices are well defined uniformly in τ. By Assumptions 7(a) and 8, the true parameter θ_0 is identifiable, lies in the interior of Θ, and the matrices $A(\theta)$, $\Sigma_v(\theta)$, and $\Sigma_{\varepsilon,\tau}(\theta)$, and therefore also the Gaussian log-likelihood $\log L_T(\theta)$, are twice continuously differentiable in an open neighborhood of θ_0.

Because the model is correctly specified and identifiable, the expected Gaussian log-likelihood is uniquely maximized at θ_0. Moreover, by Assumption 7(c), the initialization affects the log-likelihood only through an asymptotically negligible term. Therefore the normalized log-likelihood based on the Kalman filter has the same limit behavior as the exact diffuse Gaussian likelihood. Standard arguments for correctly specified Gaussian state-space models then imply $\hat{\theta} \xrightarrow{p} \theta_0$.

Since $\hat{\theta}$ is an interior maximizer of the log-likelihood,

$$\left. \frac{\partial \log L_T}{\partial\theta} \right|_{\hat{\theta}} = 0. \tag{A.51}$$

A mean-value expansion around θ_0 gives

$$0 = \left. \frac{\partial \log L_T}{\partial\theta} \right|_{\theta_0} + \left. \frac{\partial^2 \log L_T}{\partial\theta\partial\theta'} \right|_{\theta_T^*} (\hat{\theta} - \theta_0), \tag{A.52}$$

where θ_T^* lies between $\hat{\theta}$ and θ_0. Rearranging yields

$$\sqrt{T}(\hat{\theta}-\theta_0) = -\left[\frac{1}{T}\left.\frac{\partial^2 \log L_T}{\partial\theta\partial\theta'}\right|_{\theta_T^*}\right]^{-1} \frac{1}{\sqrt{T}}\left.\frac{\partial \log L_T}{\partial\theta}\right|_{\theta_0}. \tag{A.53}$$

By consistency, $\theta_T^* \xrightarrow{p} \theta_0$. Further, standard likelihood theory for correctly specified Gaussian state-space models implies that the score satisfies a central limit theorem and the normalized Hessian converges in probability,

$$\frac{1}{\sqrt{T}}\left.\frac{\partial \log L_T}{\partial\theta}\right|_{\theta_0} \xrightarrow{d} \mathcal{N}(0, \Sigma_{\theta_0}), \tag{A.54}$$

and

$$-\frac{1}{T}\left.\frac{\partial^2 \log L_T}{\partial\theta\partial\theta'}\right|_{\theta_T^*} \xrightarrow{p} \Sigma_{\theta_0}, \tag{A.55}$$

where

$$\Sigma_{\theta_0} = -\lim_{T\to\infty} E\frac{1}{T}\left.\frac{\partial^2 \log L_T(\theta)}{\partial\theta\partial\theta'}\right|_{\theta_0}. \tag{A.56}$$

Under correct Gaussian specification, the information matrix equality holds, so the asymptotic covariance matrix of the score equals Σ_{θ_0}. Therefore, by Slutsky's theorem,

$$\sqrt{T}(\hat{\theta}-\theta_0) \xrightarrow{d} \mathcal{N}(0, \Sigma_{\theta_0}^{-1}), \tag{A.57}$$

which proves the theorem. □

B Algorithms

B.1 Efficient exact discrete-time estimation

The algorithm for a computational efficient ML estimation of the CAR(k) parameters proceeds as follows:

Let P be a real lower triangular matrix, with positive elements along the diagonal, such that

$$PP' = \Omega, \tag{A.58}$$

where the matrices P_{ij} $(i = 1, 2, \ldots, 2k-1, j = 1, 2, \ldots, k)$ are calculated, respectively, from the multiplication of the ith row and jth column of the matrices P and P' as follows

$$\begin{aligned}
P_{11}P'_{11} &= \Omega_{11}, & P_{k+1,2} &= \Omega_{k+1,2}(P'_{22})^{-1}, \\
P_{21} &= \Omega_{21}(P'_{11})^{-1}, & P_{k+1,3} &= (\Omega_{k+1,3} - P_{k+1,2}P'_{32})(P'_{33})^{-1}, \\
&\vdots & &\vdots \\
P_{k1} &= \Omega_{k1}(P'_{11})^{-1}, & P_{k+1,k} &= (\Omega_{k+1,k} - P_{k+1,2}P'_{k2} - \cdots \\
& & &\quad - P_{k+1,k-1}P'_{k-1,k})(P'_{kk})^{-1}, \\
&\vdots & &\vdots \\
P_{k,k-1} &= \Omega_{k,k-1}(P'_{k-1,k-1})^{-1} & & \\
&\vdots & &\vdots \\
P_{kk}P'_{kk} &= (\Omega_{k,k} - P_{k,1}P'_{k,1} - \cdots & P_{2k-1,k} &= \Omega_{2k-1,k}(P'_{kk})^{-1} \\
&\quad - P_{k,k-1}P'_{k,k-1}) & &
\end{aligned} \tag{A.59}$$

and the rest of the matrices P_{ij} $(i, j = k+1, k+2, \ldots, T)$ are computed recursively from

$$\begin{aligned}
\Omega_0 &= \Omega_{i,i} = P_{i,i-k+1}P'_{i,i-k+1} + P_{i,i-k+2}P'_{i,i-k+2} + \cdots + P_{i,i}P'_{i,i}, \\
&\qquad (i = k+1, k+2, \ldots, T), \\
\Omega_1 &= \Omega_{i+1,i} = P_{i+1,i-k+2}P'_{i+1,i-k+2} + P_{i+1,i-k+3}P'_{i+1,i-k+3} + \cdots + P_{i+1,i}P'_{i,i}, \\
&\qquad (i = k+1, k+2, \ldots, T-1), \\
&\vdots \qquad\qquad \vdots \qquad\qquad \vdots \qquad\qquad \vdots \\
\Omega_{k-1} &= \Omega_{i+k-1,i} = P_{i+k-1,i}P'_{i,i}, \qquad (i = k+1, k+2, \ldots, T-k+1).
\end{aligned} \tag{A.60}$$

Also, let the $nT \times 1$ vector $\varepsilon = [\varepsilon'_1, \cdots, \varepsilon'_T]$ be defined as

$$P\varepsilon = \eta, \tag{A.61}$$

so that

- $\mathrm{E}[\varepsilon] = 0, \quad \mathrm{E}[\varepsilon\varepsilon'] = I_{nT\times nT},$
- $\mathrm{E}[\varepsilon_{th}] = 0, \quad \mathrm{E}[\varepsilon_{th}\varepsilon'_{th}] = I_{n\times n}\ , \quad (t = 1, \ldots, T),$
- $\mathrm{E}[\varepsilon_{th}\varepsilon'_{sh}] = 0\ , \quad (s \neq t; s, t = 1, \ldots, T).$

Then, minus twice the logarithm of the likelihood function L (ignoring the constant) is given by

$$\mathcal{L}(\theta, \Sigma) = \sum_{i=1}^{nT}(\varepsilon_i^2 + 2\log p_{ii}), \tag{A.62}$$

where p_{ii} is the ith diagonal element of P and the nT elements ε_i are computed in T vectors of size n using recursively the following procedure

$$
\begin{aligned}
\varepsilon_1 &= \left(\varepsilon_{11}, \ldots, \varepsilon_{1n}\right)' = P_{11}^{-1}\eta_1, \\
\varepsilon_2 &= \left(\varepsilon_{21}, \ldots, \varepsilon_{2n}\right)' = P_{22}^{-1}(\eta_2 - P_{21}\varepsilon_1), \\
&\vdots \qquad\qquad \vdots \qquad\qquad \vdots \\
\varepsilon_k &= \left(\varepsilon_{k1}, \ldots, \varepsilon_{kn}\right)' = P_{k,k}^{-1}(\eta_k - P_{k,k-1}\varepsilon_{k-1} - \cdots - P_{k,1}\varepsilon_1), \\
\varepsilon_{k+1} &= \left(\varepsilon_{k+1,1}, \ldots, \varepsilon_{k+1,n}\right)' = P_{k+1,k+1}^{-1}(\eta_{k+1} - P_{k+1,k}\varepsilon_k - \cdots - P_{k+1,2}\varepsilon_2), \\
&\vdots \qquad\qquad \vdots \qquad\qquad \vdots \\
\varepsilon_T &= \left(\varepsilon_{T,1}, \ldots, \varepsilon_{T,n}\right)' = P_{T,T}^{-1}(\eta_T - P_{T,T-1}\varepsilon_{T-1} - \cdots - P_{T,1}\varepsilon_{T-k+1}).
\end{aligned}
\tag{A.63}
$$

Therefore, the Gaussian estimates ($\hat{\theta}$ and $\hat{\Sigma}$) are obtained by optimizing (A.62) which, as mentioned above, due to fact of taking into account the sparse nature of Ω and also the convergence of the sequence of matrices $\bar{P}_t = (P_{tt}, P_{t,t-1}, \cdots, P_{t,t-k+1})$ $(t = k+1, k+2, \cdots, T)$, is efficient.

The optimization procedure can thus be summarized as follows:

(i) Provide initial values for A and Σ.

(ii) Compute the Hamiltonian Θ and its matrix exponential $e^{\Theta h}$. Extract F and compute Ω_ε together with Ω_{tj} $(t = 1, \cdots, 2k-1, j = 0, \cdots, k-1)$ and Ω_j $(j = 0, \cdots, k-1)$, from their specifications as given in Lemma 3.

(iii) Given these numerical representations, compute the Cholesky factorization of the matrix Ω (the matrix P).

(iv) For the minimization of $\mathcal{L}$, with this data and allowing the model's parameters to vary, obtain ε recursively as in (A.63).

(v) Plug P and the new ε into (A.62) and calculate $\mathcal{L}$.

(vi) Repeat steps (iv) and (v) until a minimum is achieved and take those $\hat{\theta}$ and $\hat{\Sigma}$ as the elements that minimize $\mathcal{L}$.

B.2 Kalman filter for i.i.d. errors

After the Kalman filter is initialized with $a_0 = [x_1', 0, \ldots, 0]'$ and $P_0 = 1000 \cdot I_{nk}$, we recursively run through the following steps:

1. Compute prediction errors
$$v_\tau = y_\tau - Z_\tau a_\tau.$$

2. Compute prediction error covariance
$$F_\tau = \Sigma_v + Z_\tau \, P_\tau \, Z'_\tau.$$

3. Update the log-likelihood function
$$L_\tau(\theta) = L_{\tau-1}(\theta) + \ln |F_\tau| + v'_\tau F_\tau^{-1} v_\tau.$$

4. Compute the Kalman gain
$$K_\tau = P_\tau Z'_\tau F_\tau^{-1}.$$

5. Discretize the model for duration δ_τ. Determine Ω_ϵ and $e^{A\delta_\tau}$ together by applying Theorem 1 in Van Loan (1978). Build the Hamiltonian matrix
$$\Theta = \begin{pmatrix} -A & \Sigma^* \\ 0 & A' \end{pmatrix},$$
and compute
$$e^{\Theta \delta_\tau} = \begin{pmatrix} F^{-1} & F^{-1}\Omega_\epsilon \\ 0 & F' \end{pmatrix}.$$
Update the state vector
$$a_{\tau+1} = e^{A\delta_\tau}(a_\tau + K_\tau v_\tau).$$

6. Update the state covariance matrix
$$P_{\tau+1} = e^{A\delta_\tau} \left(\left(I_{nk} - K_\tau Z_\tau \right) P_\tau \right) e^{A\delta'_\tau} + \Omega_\epsilon.$$

B.3 Kalman filter for MA(1) errors

For notational convenience, we assume an equally spaced time grid. Extending the analysis to tick time is straightforward. Relative to the i.i.d. case, the main change is an enlarged state space. Assume that the measurement error follows a vector MA(1) process:
$$x_{th} = Z y_{th} + v_{th}, \qquad v_{th} = e_{th} + \Theta e_{th-h}, \qquad e_{th} \sim N(0, \Sigma_{ev}),$$
where $x_{th} \in \mathbb{R}^n$, $y_{th} \in \mathbb{R}^{nk}$, $\Theta \in \mathbb{R}^{n\times n}$, and
$$Z = \begin{bmatrix} I_n & 0_{n\times n(k-1)} \end{bmatrix} \in \mathbb{R}^{n\times nk}.$$

The transition equation remains

$$y_{th} = e^{Ah} y_{th-h} + \epsilon_{th}, \qquad \epsilon_{th} \sim N(0, \Omega_\epsilon),$$

with $e^{Ah} \in \mathbb{R}^{nk \times nk}$ and $\Omega_\epsilon \in \mathbb{R}^{nk \times nk}$.

We define the augmented state

$$Y_{th} = \begin{pmatrix} y_{th} \\ e_{th} \\ \omega_{th} \end{pmatrix}, \qquad \omega_{th} = e_{th-h},$$

so that $Y_{th} \in \mathbb{R}^{nk+2n}$. The augmented transition equation is

$$Y_{th} = T_a Y_{th-h} + \upsilon_{th}, \qquad \upsilon_{th} \sim N(0, Q_a),$$

with

$$T_a = \begin{pmatrix} e^{Ah} & 0 & 0 \\ 0 & 0 & 0 \\ 0 & I_n & 0 \end{pmatrix}, \qquad Q_a = \begin{pmatrix} \Omega_\epsilon & 0 & 0 \\ 0 & \Sigma_{ev} & 0 \\ 0 & 0 & 0 \end{pmatrix}.$$

The measurement equation becomes

$$x_{th} = Z_a Y_{th}, \qquad Z_a = \begin{pmatrix} Z & I_n & \Theta \end{pmatrix} \in \mathbb{R}^{n \times (nk+2n)}.$$

There is no separate measurement noise term.

The Kalman filter is initialized with $a_0 \in \mathbb{R}^{nk+2n}$ and

$$P_0 = 1000 \cdot I_{nk+2n}.$$

For an equally spaced grid, the discretized parameters e^{Ah} and Ω_ϵ are computed once prior to filtering, using the Van Loan theorem.

At each step:

1. Compute the prediction error
$$v_{th} = x_{th} - Z_a a_{th}.$$

2. Compute its covariance
$$F_{th} = Z_a P_{th} Z_a'.$$

3. Update the log-likelihood

$$L_{th}(\theta) = L_{th-h}(\theta) + \ln|F_{th}| + v_{th}' F_{th}^{-1} v_{th},$$

up to an additive constant.

4. Compute the Kalman gain
$$K_{th} = P_{th} Z_a' F_{th}^{-1}.$$

5. Update the predicted state
$$a_{th+h} = T_a(a_{th} + K_{th} v_{th}).$$

6. Update the predicted covariance
$$P_{th+h} = T_a\big((I_{nk+2n} - K_{th} Z_a) P_{th}\big) T_a' + Q_a.$$

B.4 Kalman filter for endogenous MA(1) errors

To allow for moving-average measurement errors and contemporaneous correlation between the state innovation and the measurement innovation, consider the state-space system

$$x_{th} = Z y_{th} + e_{th} + \Theta e_{th-h},$$

$$y_{th} = F y_{th-h} + \epsilon_{th},$$

where $x_{th} \in \mathbb{R}^n$ denotes the observed process, $y_{th} \in \mathbb{R}^{nk}$ the latent state vector, and $F \in \mathbb{R}^{nk \times nk}$ the transition matrix. The measurement matrix is $Z \in \mathbb{R}^{n \times nk}$, and $\Theta \in \mathbb{R}^{n \times n}$ governs the MA(1) structure in the measurement equation.

The innovations satisfy
$$\begin{pmatrix} \epsilon_{th} \\ e_{th} \end{pmatrix} \sim N\left(0, \begin{pmatrix} Q & S \\ S' & \Sigma_e \end{pmatrix}\right),$$

where $Q \in \mathbb{R}^{nk \times nk}$ is the covariance matrix of the state innovation, $\Sigma_e \in \mathbb{R}^{n \times n}$ is the covariance matrix of the contemporaneous measurement innovation, and $S \in \mathbb{R}^{nk \times n}$ is the contemporaneous cross-covariance matrix. In the present specification, only the first n components of the state innovation are allowed to be correlated with the measurement innovation, so that
$$S = \begin{pmatrix} S_0 \\ 0 \end{pmatrix}, \qquad S_0 \in \mathbb{R}^{n \times n}.$$

To obtain a standard linear Gaussian state-space representation, define the augmented state vector
$$\alpha_{th} = \begin{pmatrix} y_{th} \\ e_{th} \\ e_{th-h} \end{pmatrix} \in \mathbb{R}^{nk+2n}.$$

Then the model can be written as

$$\alpha_{th} = T_a \alpha_{th-h} + \eta_{th}, \qquad x_{th} = Z_a \alpha_{th},$$

with transition matrix

$$T_a = \begin{pmatrix} F & 0 & 0 \\ 0 & 0 & 0 \\ 0 & I_n & 0 \end{pmatrix},$$

measurement matrix

$$Z_a = \begin{pmatrix} Z & I_n & \Theta \end{pmatrix},$$

and state disturbance

$$\eta_{th} = \begin{pmatrix} \epsilon_{th} \\ e_{th} \\ 0 \end{pmatrix}, \qquad \mathrm{Var}(\eta_{th}) = Q_a,$$

where

$$Q_a = \begin{pmatrix} Q & S & 0 \\ S' & \Sigma_e & 0 \\ 0 & 0 & 0 \end{pmatrix}.$$

Given initial values a_h and P_h, the Kalman filter proceeds recursively for $t = 1, \ldots, T$ as follows:

1. Compute prediction errors
$$v_{th} = x_{th} - Z_a a_{th}.$$

2. Compute prediction error covariance
$$F_{th} = Z_a P_{th} Z_a'.$$

3. Update the log-likelihood function
$$L_{th}(\theta) = L_{th-h}(\theta) + \ln |F_{th}| + v_{th}' F_{th}^{-1} v_{th}.$$

4. Compute the Kalman gain
$$K_{th} = P_{th} Z_a' F_{th}^{-1}.$$

5. Update the state vector
$$a_{th+h} = T_a (a_{th} + K_{th} v_{th}).$$

6. Update the state covariance matrix

$$P_{th+h} = T_a\Big(\left(I_{nk+2n} - K_{th}Z_a\right)P_{th}\left(I_{nk+2n} - K_{th}Z_a\right)'\Big)T_a' + Q_a.$$

C Additional simulation results

C.1 Asymptotic distribution

Figure C.1: Asymptotic distribution of the standardized continuous information share. The theoretical standard normal distribution is drawn as a black solid line.

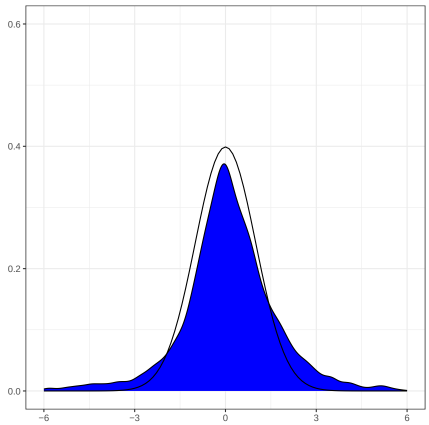

(a) $N = 100$, $h = 1$

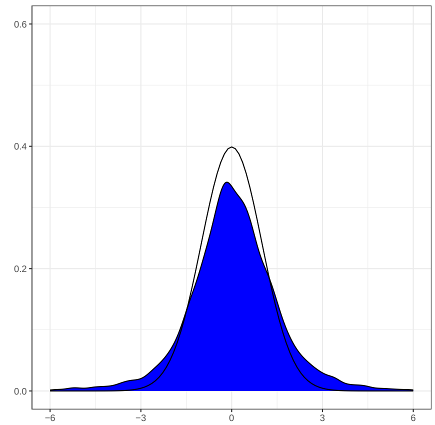

(b) $N = 200$, $h = 1$

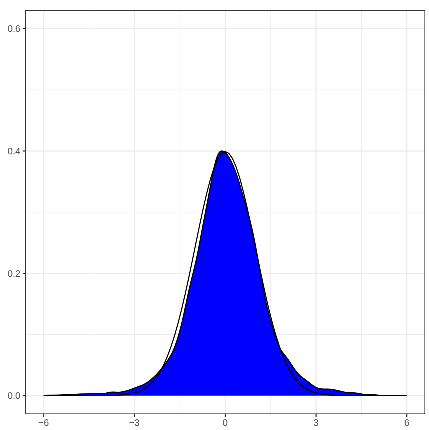

(c) $N = 100$, $h = 1/2$

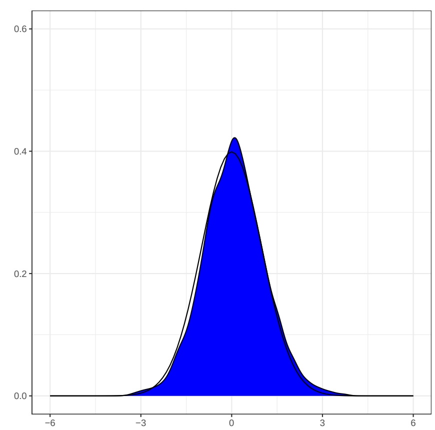

(d) $N = 200$, $h = 1/2$

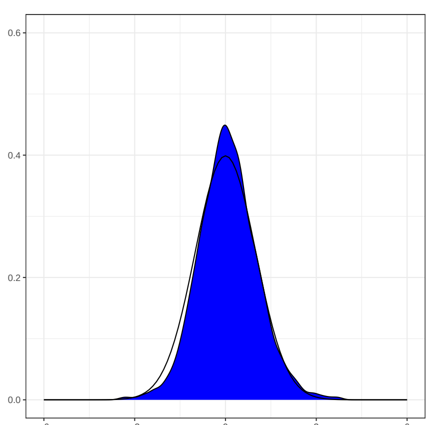

(e) $N = 100$, $h = 1/4$

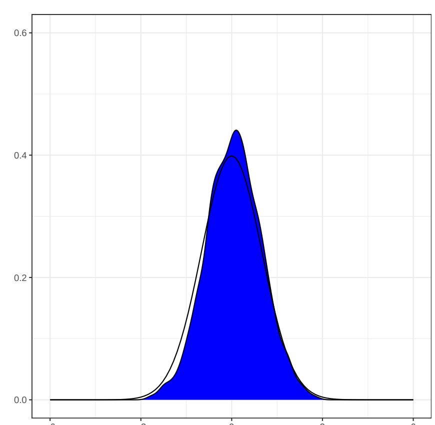

(f) $N = 200$, $h = 1/4$

C.2 Size and power of diagonality tests

Table C.1: Empirical size and power of the Wald test

		Size			Power I			Power II		
		$\rho = 0$			$\rho = 0.25$			$\rho = 0.5$		
	h	10%	5%	1%	10%	5%	1%	10%	5%	1%
$N = 100$	1	0.004	0.001	0.001	0.023	0.018	0.010	0.188	0.113	0.050
	1/2	0.029	0.014	0.002	0.463	0.298	0.091	0.993	0.979	0.893
	1/4	0.067	0.030	0.002	0.976	0.955	0.829	1.000	1.000	1.000
	1/8	0.075	0.037	0.004	1.000	1.000	1.000	1.000	1.000	1.000
	1/16	0.081	0.037	0.009	1.000	1.000	1.000	1.000	1.000	1.000
$N = 200$	1	0.000	0.000	0.000	0.025	0.010	0.004	0.425	0.229	0.056
	1/2	0.020	0.009	0.002	0.844	0.687	0.297	1.000	1.000	0.999
	1/4	0.051	0.024	0.000	1.000	1.000	0.995	1.000	1.000	1.000
	1/8	0.071	0.022	0.007	1.000	1.000	1.000	1.000	1.000	1.000
	1/16	0.076	0.029	0.007	1.000	1.000	1.000	1.000	1.000	1.000

Note: The Wald test is conducted after estimating a CAR(k) model using the unconstrained likelihood. We simulate data for a two market system with the parameters of our main specification.

C.3 Exact discretization: additional simulations

Table C.2: Simulation results for the HIS based on a VECM with different lag lengths

	N = 100				N = 200			
h	T	$k=1$	$k=2$	$k=\sqrt{T}$	T	$k=1$	$k=2$	$k=\sqrt{T}$
1	100	−0.070	−0.062	−0.127	200	−0.062	−0.048	−0.092
		(0.134)	(0.158)	(0.266)		(0.094)	(0.115)	(0.220)
1/2	200	−0.055	−0.020	−0.073	400	−0.040	−0.006	−0.037
		(0.114)	(0.134)	(0.230)		(0.080)	(0.092)	(0.187)
1/4	400	−0.054	0.001	−0.039	800	−0.050	0.008	−0.020
		(0.100)	(0.119)	(0.197)		(0.072)	(0.085)	(0.162)
1/8	800	−0.062	0.007	−0.022	1600	−0.066	0.013	−0.024
		(0.093)	(0.112)	(0.177)		(0.068)	(0.080)	(0.142)
1/16	1600	−0.078	0.009	−0.028	3200	−0.071	0.012	−0.018
		(0.092)	(0.112)	(0.159)		(0.063)	(0.081)	(0.133)

The table reports the bias (average deviation from the true value) and the standard deviation in parentheses for 1,000 draws. All values are reported for the first market. The standard deviations for the second market are identical and the bias is identical up to a sign switch. The true values for the continuous-time information share are (0.8, 0.2).

Table C.3: Simulation results for equal information shares

	N = 100				N = 200			
h	T	$\alpha_{h,\perp,1}$	HIS_1	IS_1^c	T	$\alpha_{h,\perp,1}$	HIS_1	IS_1^c
1	100	−0.003	−0.003	0.000	200	−0.003	−0.006	0.000
		(0.117)	(0.176)	(0.181)		(0.079)	(0.127)	(0.131)
1/2	200	−0.003	−0.006	0.001	400	0.001	0.003	0.013
		(0.087)	(0.155)	(0.158)		(0.059)	(0.110)	(0.114)
1/4	400	0.002	0.004	0.016	800	0.002	0.005	0.018
		(0.073)	(0.136)	(0.150)		(0.051)	(0.098)	(0.108)
1/8	800	0.003	0.006	0.022	1600	−0.001	−0.001	0.013
		(0.067)	(0.126)	(0.145)		(0.048)	(0.093)	(0.107)
1/16	1600	−0.002	−0.003	0.010	3200	0.001	0.002	0.015
		(0.064)	(0.122)	(0.145)		(0.043)	(0.084)	(0.101)

The table reports the bias (average deviation from the true value) and the standard deviation in parentheses for 1,000 draws. All values are reported for the first market. The standard deviations for the second market are identical and the bias is identical up to a sign switch. The true values for the continuous-time information share are (0.5, 0.5). The CS and HIS are computed from a VECM(1). The IS^c is based on an unconstrained likelihood.

C.4 Exact discretization: off-diagonal elements in A_1

For this simulation experiment, we use the same parameters as in the main paper except that we now change the off-diagonal element of A_1 so that

$$A_1 = \begin{bmatrix} -3 & A_{1,21} \\ A_{1,21} & -3 \end{bmatrix}, \tag{A.64}$$

and $A_{1,21}$ is set to either 1 or 2. Putting nonzero off-diagonal elements on the A_1 matrix leads to a much higher contemporaneous correlation of η_{th} for the aggregated time series. The value of the true continuous-time information share remains unchanged. A change in A_1 only alters the scaling factor of $A(\infty)$ in a two-market system which is irrelevant when IS^c is computed. The CAR(k) model allows us to induce error term correlation by changing the off-diagonal elements of A_1 from zero to nonzero while keeping Σ diagonal. This means for the continuous-time model that the aggregation effect leads to a higher contemporaneous correlation at longer sample intervals. Figure C.2 displays the change in the correlation structure for different choices of $A_{1,21}$. The values depicted in the figures can be directly computed from the Ω_0 matrix.

Figure C.2: Contemporaneous correlation of η_{th}
This figure depicts the effects of temporal aggregation on the contemporaneous correlation of η_{th} for different choices of the off-diagonal elements of A_1. The x-axis is represented on a logarithmic scale.

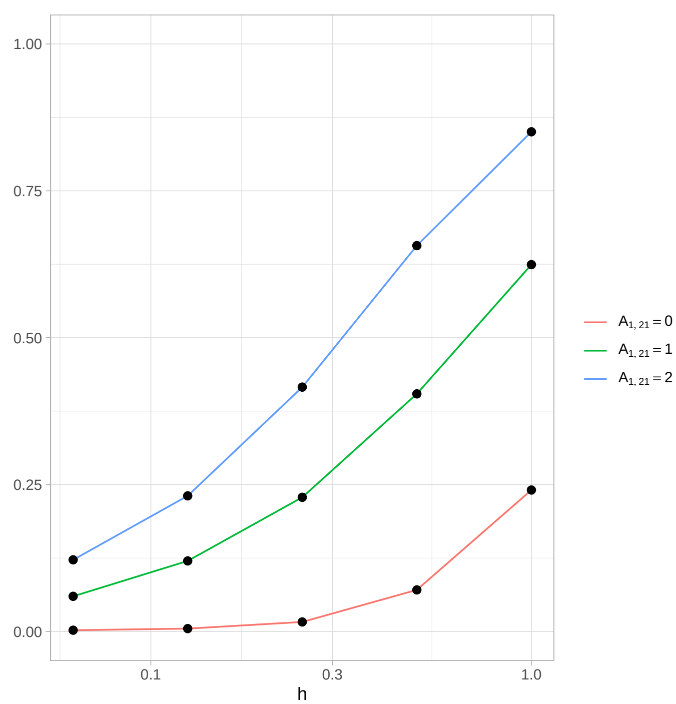

These results show that the model can generate cointegrated price data with uncorrelated continuous-time innovations but correlated discrete-time innovations. It is therefore not necessary to use ultra-high-frequency data to identify market-specific contributions to efficient price variance. By imposing a diagonal covariance matrix, we can accurately estimate the market-specific variances at relatively low frequencies and obtain an order-invariant information share, while still allowing for substantial correlation in the exact discrete-time innovations. This contrasts with the high-resolution VECM of Hasbrouck (2021), which relies on ultra-high-frequency observations to reduce contemporaneous correlation in the innovations.

The performance of the price discovery measures in the non-zero off-diagonal setting with $A_{1,21} = \{1, 2\}$ is evaluated in Table C.4. While the relative performance does not change with respect to the benchmark results reported in Table 1 in the main paper, additional noise in the system increases the sampling error.

Table C.4: Simulation results for nonzero off-diagonals in the CAR(2) model

			$A_{1,21} = 1$					
		$N = 100$				$N = 200$		
h	T	$\alpha_{h,\perp,1}$	HIS_1	IS_1^c	T	$\alpha_{h,\perp,1}$	HIS_1	IS_1^c
1	100	0.118	−0.117	−0.047	200	0.114	−0.109	−0.021
		(0.223)	(0.120)	(0.138)		(0.153)	(0.088)	(0.095)
1/2	200	0.051	−0.075	−0.021	400	0.059	−0.059	0.001
		(0.138)	(0.122)	(0.120)		(0.089)	(0.079)	(0.078)
1/4	400	0.015	−0.056	−0.005	800	0.011	−0.053	0.003
		(0.096)	(0.110)	(0.113)		(0.068)	(0.080)	(0.076)
1/8	800	−0.012	−0.061	−0.003	1600	−0.016	−0.059	0.003
		(0.082)	(0.109)	(0.109)		(0.055)	(0.077)	(0.075)
1/16	1600	−0.028	−0.068	−0.006	3200	−0.031	−0.067	0.003
		(0.072)	(0.106)	(0.110)		(0.051)	(0.077)	(0.074)
			$A_{1,21} = 2$					
		$N = 100$				$N = 200$		
h	T	$\alpha_{h,\perp,1}$	HIS_1	IS_1^c	T	$\alpha_{h,\perp,1}$	HIS_1	IS_1^c
1	100	0.345	−0.174	−0.042	200	0.337	−0.166	−0.021
		(0.423)	(0.626)	(0.143)		(0.278)	(0.064)	(0.107)
1/2	200	0.163	−0.113	−0.027	400	0.176	−0.096	−0.002
		(0.230)	(0.112)	(0.134)		(0.156)	(0.078)	(0.089)
1/4	400	0.072	−0.068	−0.008	800	0.067	−0.063	0.000
		(0.145)	(0.119)	(0.122)		(0.100)	(0.086)	(0.085)
1/8	800	0.016	−0.060	−0.006	1600	0.009	−0.061	−0.005
		(0.108)	(0.120)	(0.116)		(0.076)	(0.089)	(0.083)
1/16	1600	−0.017	−0.070	−0.017	3200	−0.013	−0.058	−0.002
		(0.090)	(0.121)	(0.119)		(0.061)	(0.084)	(0.082)

The table reports the bias (average deviation from the true value) and the standard deviation in parentheses for 1,000 draws. All values are reported for the first market. The standard deviations for the second market are identical and the bias is identical up to a sign switch. The true values for the continuous-time information share are (0.8, 0.2). The CS and HIS are computed from a VECM(1). The IS^c is based on an unconstrained likelihood. Similar results are obtained from a constrained likelihood.

C.5 Exact discretization: CAR(3) results

In this experiment, we turn to a different higher-order model specification, setting $k = 3$. Note that the CAR(2) process is not nested in the CAR(3) process. Hence, parametrizations that satisfy Assumption 6 can be quite different from the main specification used for the CAR(2) experiments. Here, we generate data according to the following model: $\alpha = (-100, 200)'$, $\beta = (1, -1)'$,

$$A_1 = \begin{bmatrix} -300 & 0 \\ 0 & -300 \end{bmatrix}, \quad A_2 = \begin{bmatrix} -10 & 0 \\ 0 & -10 \end{bmatrix}, \quad \Sigma = \begin{bmatrix} 100 & 0 \\ 0 & 100 \end{bmatrix}. \tag{A.65}$$

Again, the true continuous-time information shares are (0.8, 0.2) and the results can be compared with the CAR(2) results. As expected, changing the values for A_2 does not affect the performance of the continuous-time information share measure but can influence the performance of the component shares and the HIS as it changes the MA structure of the process in discrete time.

The results are reported in Table C.5. The continuous-time information share does not show any bias for all combinations of N and h. The standard deviations first decrease when the sampling frequency increases and then increase again when the speed of adjustment in the discrete-time model becomes too small. The component share and the HIS are biased and inconsistent since the MA(2) structure of the error terms is ignored in the simple VECM(2). The standard deviations are substantially larger than those for the continuous-time information share at more extreme values of h.

The corresponding results for equal information shares, setting $\alpha = (-100, 100)'$, are reported in Table C.6. In this setting, the component shares and the HIS are not biased but the standard deviations are much larger than those for the continuous-time information share. Again, these results highlight that the continuous-time information share is a more efficient alternative at high frequencies and provides a data-coherent estimation framework.

Table C.5: Simulation results for the CAR(3) model

h	T	$N=100$ $\alpha_{h,\perp,1}$	HIS_1	IS_1^c	T	$N=200$ $\alpha_{h,\perp,1}$	HIS_1	IS_1^c
1	100	0.001	−0.111	0.020	200	−0.002	−0.098	0.010
		(0.182)	(0.161)	(0.104)		(0.119)	(0.117)	(0.095)
1/2	200	−0.002	−0.059	−0.016	400	0.003	−0.042	0.002
		(0.116)	(0.138)	(0.124)		(0.076)	(0.093)	(0.082)
1/4	400	0.011	−0.015	−0.005	800	0.007	−0.010	−0.007
		(0.089)	(0.116)	(0.132)		(0.063)	(0.083)	(0.103)
1/8	800	0.045	0.035	−0.007	1600	0.041	0.042	−0.005
		(0.094)	(0.113)	(0.098)		(0.066)	(0.082)	(0.073)
1/16	1600	0.092	0.057	−0.011	3200	0.090	0.077	−0.008
		(0.145)	(0.150)	(0.104)		(0.106)	(0.105)	(0.081)

The table reports the bias (average deviation from the true value) and the standard deviation in parentheses for 1,000 draws. All values are reported for the first market. The standard deviations for the second market are identical and the bias is identical up to a sign switch. The true values for the continuous-time information share are (0.8, 0.2). The CS and HIS are computed from a VECM(2).

Table C.6: Simulation results for equal information shares, CAR(3)

h	T	$N=100$ $\alpha_{h,\perp,1}$	HIS_1	IS_1^c	T	$N=200$ $\alpha_{h,\perp,1}$	HIS_1	IS_1^c
1	100	−0.005	−0.006	0.008	200	−0.003	−0.003	−0.021
		(0.165)	(0.204)	(0.184)		(0.110)	(0.149)	(0.147)
1/2	200	−0.005	−0.007	−0.008	400	0.005	0.008	0.009
		(0.118)	(0.183)	(0.192)		(0.078)	(0.131)	(0.136)
1/4	400	0.006	0.011	0.019	800	0.002	0.005	0.003
		(0.098)	(0.171)	(0.197)		(0.069)	(0.125)	(0.154)
1/8	800	0.004	0.008	0.005	1600	0.003	0.005	0.004
		(0.108)	(0.192)	(0.154)		(0.075)	(0.142)	(0.113)
1/16	1600	0.001	0.003	0.001	3200	0.001	0.002	0.000
		(0.169)	(0.265)	(0.166)		(0.122)	(0.210)	(0.133)

The table reports the bias (average deviation from the true value) and the standard deviation in parentheses for 1,000 draws. All values are reported for the first market. The standard deviations for the second market are identical and the bias is identical up to a sign switch. The true values for the continuous-time information share are (0.5, 0.5). The CS and HIS are computed from a VECM(2).

C.6 Exact discretization: five-market system

In this experiment, we extend our model to a five-market system. To do so, we set $\Sigma = I_5$, $\beta' = (I_r, -\iota_r)$, where $r = n - 1$,

$$\alpha = \begin{bmatrix} -2 & -2 & -2 & -2 \\ 2 & 0 & 0 & 0 \\ 0 & 2 & 0 & 0 \\ 0 & 0 & 2 & 0 \\ 0 & 0 & 0 & 2 \end{bmatrix}, \tag{A.66}$$

and $A_1 = diag(-3, \ldots, -3)$. The information shares in this system are equal for all markets. Since the number of covariance terms in Σ is quite large and in contrast to the simulations for a two-market system, we impose the diagonality assumption for the estimation. The results for $N = 400$ and $N = 800$ are reported in Table C.7.

Table C.7: Simulation results for equal information shares in a five market system

	$N = 400$						$N = 800$					
h	T	y_1	y_2	y_3	y_4	y_5	T	y_1	y_2	y_3	y_4	y_5
1	400	0.095	−0.019	−0.029	−0.037	−0.010	800	0.100	−0.020	−0.034	−0.037	−0.009
		(0.029)	(0.046)	(0.044)	(0.042)	(0.046)		(0.026)	(0.043)	(0.042)	(0.042)	(0.044)
1/2	800	−0.021	0.016	0.006	−0.027	0.026	1600	−0.019	0.010	−0.001	−0.024	0.035
		(0.029)	(0.068)	(0.082)	(0.051)	(0.084)		(0.027)	(0.064)	(0.077)	(0.046)	(0.091)
1/4	1600	−0.063	−0.013	0.033	−0.001	0.044	3200	−0.063	−0.008	0.030	−0.004	0.045
		(0.020)	(0.060)	(0.077)	(0.067)	(0.074)		(0.019)	(0.060)	(0.081)	(0.059)	(0.074)
1/8	3200	−0.063	−0.018	0.040	0.001	0.041	6400	−0.062	−0.023	0.039	0.006	0.039
		(0.019)	(0.061)	(0.082)	(0.063)	(0.081)		(0.018)	(0.062)	(0.078)	(0.068)	(0.076)

The table reports the bias (average deviation from the true value) and the standard deviation in parentheses for 1,000 draws. The true values for the continuous-time information share are (0.2, 0.2, 0.2, 0.2, 0.2). The IS^c is based on a constrained likelihood.

There is no sensible way of comparing the IS^c results with the HIS as we would have to compute it for many orderings and we cannot impose the diagonality assumption directly. Consequently, we do not compare our results to the discrete-time alternatives. We observe that the standard deviations improve only slightly from $h = 1$ to $h = 1/8$ and also doubling N seems to only have a marginal effect on bias and variance. The reduced precision can be attributed to a proliferation of parameters which makes the numerical optimization of the likelihood much more difficult. In the next subsection, we investigate whether the information shares for a subset of a larger system can be accurately estimated. The motivation for this analysis is that financial markets are heavily fragmented and not every market can be taken into consideration due to limited data availability and increasing computational costs.

C.7 Subsetting a larger system (discrete-time)

We generate data from a five-variable systems and estimate the information shares in discrete time for a subset of the variables. This is done to investigate whether our analysis can accurately determine the leading market in a two-variable system although the price discovery process happens in a larger system. We specify the VECM

$$\Delta p_t = \Pi p_{t-1} + \sum_{i=1}^{K-1} \Gamma_i \Delta p_{t-i} + u_t, \tag{A.67}$$

with $K = 2$, $\Gamma_1 = -0.1 I_5$ and

$$\beta' = \begin{bmatrix} 1 & 0 & 0 & 0 & -1 \\ 0 & 1 & 0 & 0 & -1 \\ 0 & 0 & 1 & 0 & -1 \\ 0 & 0 & 0 & 1 & -1 \end{bmatrix}. \tag{A.68}$$

Using this structure guarantees that both models are driven by one common stochastic trend. We impose equal information shares for all variables by setting the adjustment coefficient matrix to

$$\alpha = \begin{bmatrix} -0.2 & 0 & 0 & 0 \\ 0 & -0.2 & 0 & 0 \\ 0 & 0 & -0.2 & 0 \\ 0 & 0 & 0 & -0.2 \\ 0.2 & 0.2 & 0.2 & 0.2 \end{bmatrix} \tag{A.69}$$

and setting the error term covariance matrix to a diagonal matrix with equal variance, the identity matrix in our case. From this system, we only select the first two variables and compute their information share. The true value is (0.5,0.5) in this system. We vary the sample size T and consider either a diagonal covariance matrix (I_5) or the non-diagonal covariance matrix

$$V = \begin{pmatrix} 1 & 0.2 & 0.5 & 0.3 & 0.1 \\ 0.2 & 1 & 0.4 & 0.2 & 0.1 \\ 0.5 & 0.4 & 1 & 0.6 & 0.2 \\ 0.3 & 0.2 & 0.6 & 1 & 0.3 \\ 0.1 & 0.1 & 0.2 & 0.3 & 1 \end{pmatrix}.$$

The results are reported in Table C.8 and show that the contributions of both markets can be accurately determined if a smaller subset is selected.

Table C.8: Simulation results for a subset of the $n = 5$ system (discrete-time)

	diagonal		non-diagonal	
T	HIS_1	$\overline{HIS}_1$	HIS_1	$\overline{HIS}_1$
100	0.562	0.055	0.570	0.168
	(0.139)	(0.042)	(0.158)	(0.068)
200	0.564	0.045	0.577	0.171
	(0.117)	(0.034)	(0.133)	(0.055)
400	0.567	0.034	0.577	0.174
	(0.088)	(0.027)	(0.100)	(0.044)
800	0.568	0.025	0.579	0.175
	(0.066)	(0.019)	(0.077)	(0.033)

The table reports the mean HIS value and the standard deviation in parentheses for 1,000 draws. $\overline{HIS}$ denotes the average spread. All values are reported for the first market.

C.8 Subsetting a larger system (continuous-time)

In this subsection, we repeat the previous analysis subsetting a $n = 5$ system in continuous time. The DGP is the same as the one used to generate Table A4 in the main paper. In Table C.9, we specify a diagonal and non-diagonal covariance, respectively. In both specifications, we find that the bias and the standard deviation of the continuous-time information share reduces if we follow the convergence path in mixed asymptotics. The asymptotic behaviour of the discrete-time measures is comparable to the results obtained in the main paper. In summary, it appears sensible to reduce a larger price system to a smaller subsystem and thereby also reducing the computational cost. The relative importance of markets can still be determined with high accuracy.

C.9 Single trading day estimation

In this simulation, we generate data for a single trading day mimicking the data structure in the empirical application. For the discrete-time measures (CS and HIS), we adjust the model specification for each discretization parameter. Similar to the high-resolution VECM, we increase the number of lags with the sampling frequency to cover the same time scale. For the first discretization choice of $h = 1/100$, we estimate a VECM(1), continue with a VECM(2) for $h = 1/200$ and double the lag length for each doubling of the sample size. CS and HIS do not seem to gain any precision from the higher sampling frequency. Both measures are substantially biased. In contrast, the bias of the continuous-time information shares seems to vanish for higher sampling frequencies. Considering that 1-second data yields a discretization parameter of $h = 1/22500$, the simulation results show that the temporal aggegation bias should not play a major role in our empirical application.

These simulation results can guide us in selecting one measure if HIS and IS^c disagree.

Table C.9: Simulation results for a subset of the $n = 5$ system (continuous-time)

					diagonal			
		$N = 100$				$N = 200$		
h	T	$\alpha_{h,\perp,1}$	HIS_1	IS_1^c	T	$\alpha_{h,\perp,1}$	HIS_1	IS_1^c
1	100	0.060	0.117	−0.096	200	0.022	0.050	−0.032
		(0.128)	(0.201)	(0.206)		(0.091)	(0.164)	(0.163)
1/2	200	0.022	0.050	−0.032	400	0.022	0.049	−0.040
		(0.091)	(0.164)	(0.163)		(0.065)	(0.121)	(0.122)
1/4	400	−0.004	−0.001	−0.038	800	0.001	0.009	−0.024
		(0.078)	(0.145)	(0.161)		(0.053)	(0.105)	(0.118)
1/8	800	−0.009	−0.014	−0.032	1600	−0.009	−0.014	−0.027
		(0.069)	(0.132)	(0.157)		(0.049)	(0.096)	(0.114)
1/16	1600	−0.014	−0.026	0.034	3200	−0.013	−0.024	−0.028
		(0.066)	(0.126)	(0.154)		(0.045)	(0.088)	(0.107)
					non-diagonal			
		$N = 100$				$N = 200$		
h	T	$\alpha_{h,\perp,1}$	HIS_1	IS_1^c	T	$\alpha_{h,\perp,1}$	HIS_1	IS_1^c
1	100	0.057	0.077	−0.103	200	0.063	0.087	−0.138
		(0.171)	(0.188)	(0.213)		(0.113)	(0.137)	(0.172)
1/2	200	0.018	0.031	−0.055	400	0.022	0.034	−0.058
		(0.125)	(0.158)	(0.164)		(0.092)	(0.121)	(0.128)
1/4	400	−0.003	−0.001	−0.036	800	−0.001	0.003	−0.033
		(0.111)	(0.144)	(0.160)		(0.073)	(0.099)	(0.111)
1/8	800	−0.011	−0.014	−0.025	1600	−0.010	−0.012	−0.031
		(0.095)	(0.125)	(0.145)		(0.067)	(0.091)	(0.107)
1/16	1600	−0.014	−0.019	−0.020	3200	−0.010	−0.012	−0.020
		(0.090)	(0.120)	(0.137)		(0.061)	(0.083)	(0.098)

The table reports the bias (average deviation from the true value) and the standard deviation in parentheses for 1,000 draws. All values are reported for the first market. The standard deviations for the second market are identical and the bias is identical up to a sign switch. The true values for the continuous time information share are (0.5, 0.5). The CS and HIS are computed from a VECM(1). The IS^c is based on an unconstrained likelihood.

Clearly both measures are imprecise if we estimate the respective model for a single trading day (the standard deviation does not change substantially from $h = 1/100$ to $h = 1/1600$ but IS^c is less biased than HIS and the bias decreases with the sampling frequency. Consequently, the results are in line with our main results for 100 and 200 trading days. This highlights that we can estimate daily continuous time information share and average them over a longer sampling period. In contrast, we should not trust the average of biased daily HIS estimates.

Table C.10: Simulation results for infill asymptotics (single trading day)

		$N=1$		
h	T	$\alpha_{h,\perp,1}$	HIS_1	IS_1^c
1/100	100	−0.158	−0.281	−0.227
		(0.381)	(0.360)	(0.347)
1/200	200	−0.166	−0.295	−0.267
		(0.380)	(0.355)	(0.365)
1/400	400	−0.160	−0.262	−0.211
		(0.382)	(0.360)	(0.326)
1/800	800	−0.159	−0.276	−0.158
		(0.382)	(0.356)	(0.292)
1/1600	1600	−0.160	−0.263	−0.111
		(0.381)	(0.360)	(0.267)

The table reports the bias (average deviation from the true value) and the standard deviation in parentheses for 1,000 draws. All values are reported for the first market. The standard deviations for the second market are identical and the bias is identical up to a sign switch. The true values for the continuous time information share are (0.8, 0.2). The CS and HIS are computed from a VECM(k) where k is successively increased with the sample size so that $k = \{1, 2, 4, 8, 16\}$. The IS^c is based on an unconstrained likelihood.

C.10 Kalman filter approach: additional simulations

Table C.11: Simulation results for the CAR(2) model

	$N=100$				$N=200$			
h	T	$\alpha_{h,\perp,1}$	HIS_1	IS_1^c	T	$\alpha_{h,\perp,1}$	HIS_1	IS_1^c
1	100	0.003	−0.064	−0.113	200	0.001	−0.055	−0.047
		(0.119)	(0.135)	(0.154)		(0.082)	(0.093)	(0.108)
1/2	200	−0.013	−0.022	−0.001	400	−0.023	−0.052	−0.025
		(0.081)	(0.112)	(0.111)		(0.058)	(0.084)	(0.084)
1/4	400	−0.035	−0.066	−0.032	800	−0.030	−0.053	−0.012
		(0.066)	(0.103)	(0.111)		(0.047)	(0.072)	(0.075)
1/8	800	−0.035	−0.064	−0.014	1600	−0.039	−0.065	−0.010
		(0.061)	(0.096)	(0.106)		(0.042)	(0.068)	(0.072)
1/16	1600	−0.044	−0.076	−0.019	3200	−0.043	−0.072	−0.006
		(0.057)	(0.093)	(0.106)		(0.040)	(0.066)	(0.053)

The table reports the bias (average deviation from the true value) and the standard deviation in parentheses for 1,000 draws. All values are reported for the first market. The standard deviations for the second market are identical and the bias is identical up to a sign switch. The true values for the continuous-time information share are (0.8, 0.2). The CS and HIS are computed from a VECM(1). Although the data are generated without microstructure noise contamination, the Kalman filter estimates a full covariance matrix for i.i.d. measurement errors.

Table C.12: Simulation results for the CAR(2) model in presence of i.i.d. microstructure noise ($\omega^2 = 0.001$)

	$N=100$				$N=200$			
h	T	$\alpha_{h,\perp,1}$	HIS_1	IS_1^c	T	$\alpha_{h,\perp,1}$	HIS_1	IS_1^c
1	100	0.004	−0.063	−0.115	200	0.003	−0.054	−0.054
		(0.119)	(0.133)	(0.156)		(0.082)	(0.093)	(0.117)
1/2	200	−0.003	−0.032	−0.028	400	−0.013	−0.039	−0.028
		(0.084)	(0.112)	(0.114)		(0.061)	(0.085)	(0.085)
1/4	400	−0.016	−0.003	−0.031	800	0.025	0.017	−0.010
		(0.091)	(0.118)	(0.114)		(0.062)	(0.079)	(0.078)
1/8	800	0.182	0.116	−0.012	1600	0.170	0.134	−0.008
		(0.162)	(0.112)	(0.091)		(0.111)	(0.077)	(0.064)
1/16	1600	0.389	0.132	−0.006	3200	0.390	0.167	−0.004
		(0.270)	(0.114)	(0.067)		(0.188)	(0.054)	(0.045)

The table reports the bias (average deviation from the true value) and the standard deviation in parentheses for 1,000 draws. All values are reported for the first market. The standard deviations for the second market are identical and the bias is identical up to a sign switch. The true values for the continuous-time information share are (0.8, 0.2). The CS and HIS are computed from a VECM(1).

Table C.13: Presence of i.i.d. market microstructure noise and in-fill asymptotics ($\rho = 0.5$)

		$\omega^2=0.001$				$\omega^2=0.0001$				$\omega^2=0$			
h	T	HIS_1	IS_1^c	ρ_u	ρ_η	HIS_1	IS_1^c	ρ_u	ρ_η	HIS_1	IS_1^c	ρ_u	ρ_η
1/100	100	−0.167	−0.114	−0.338	−0.023	−0.132	−0.031	−0.038	0.016	−0.150	−0.004	0.008	0.026
		(0.341)	(0.169)	(0.142)	(0.670)	(0.317)	(0.162)	(0.087)	(0.390)	(0.298)	(0.032)	(0.085)	(0.066)
1/200	200	−0.161	−0.060	−0.391	0.047	−0.183	−0.011	−0.166	0.030	−0.180	−0.002	0.003	0.018
		(0.346)	(0.153)	(0.097)	(0.453)	(0.327)	(0.125)	(0.064)	(0.279)	(0.302)	(0.020)	(0.055)	(0.029)
1/400	400	−0.193	−0.030	−0.435	0.039	−0.148	0.002	−0.292	0.009	−0.154	0.002	0.002	0.011
		(0.341)	(0.129)	(0.065)	(0.314)	(0.346)	(0.094)	(0.049)	(0.220)	(0.306)	(0.019)	(0.038)	(0.021)
1/800	800	−0.176	−0.010	−0.468	0.036	−0.151	0.010	−0.375	0.008	−0.150	0.003	0.001	0.008
		(0.355)	(0.098)	(0.043)	(0.229)	(0.345)	(0.079)	(0.037)	(0.174)	(0.301)	(0.018)	(0.027)	(0.017)
1/1600	1600	−0.197	−0.013	−0.484	0.034	−0.161	−0.004	−0.426	0.024	−0.155	0.003	−0.001	0.007
		(0.353)	(0.071)	(0.027)	(0.141)	(0.355)	(0.060)	(0.025)	(0.128)	(0.308)	(0.017)	(0.020)	(0.015)

The table reports the bias (average deviation from the true value) and the standard deviation in parentheses for 1,000 draws. The true values for the midpoints of the continuous-time information share are (2/3, 1/3). The HIS is computed from a VECM(k) where k is successively increased with the sample size so that $k = \{1, 2, 4, 8, 16\}$. ρ_u and ρ_η denote the estimated innovation correlation for the discrete-time and continuous-time model, respectively.

Table C.14: Presence of i.i.d. market microstructure noise and in-fill asymptotics ($\rho = 0.5$)

		$\omega^2 = (0.001, 0.005)$				$\omega^2 = (0.0001, 0.0005)$				$\omega^2 = 0$			
h	T	HIS_1	IS_1^c	ρ_u	ρ_η	HIS_1	IS_1^c	ρ_u	ρ_η	HIS_1	IS_1^c	ρ_u	ρ_η
1/100	100	0.123	−0.135	−0.431	−0.011	−0.231	−0.064	−0.459	0.005	−0.150	−0.004	0.008	0.026
		(0.209)	(0.156)	(0.116)	(0.690)	(0.332)	(0.166)	(0.115)	(0.518)	(0.298)	(0.032)	(0.085)	(0.066)
1/200	200	0.128	−0.082	−0.462	0.037	−0.248	−0.026	−0.482	0.045	−0.180	−0.002	0.003	0.018
		(0.218)	(0.154)	(0.079)	(0.535)	(0.338)	(0.130)	(0.078)	(0.354)	(0.302)	(0.020)	(0.055)	(0.029)
1/400	400	0.095	−0.049	−0.485	0.045	−0.291	−0.006	−0.492	0.018	−0.154	0.002	0.002	0.011
		(0.239)	(0.126)	(0.055)	(0.373)	(0.325)	(0.107)	(0.054)	(0.265)	(0.306)	(0.019)	(0.038)	(0.021)
1/800	800	0.063	−0.024	−0.491	0.055	−0.320	0.006	−0.492	0.015	−0.150	0.003	0.001	0.008
		(0.278)	(0.106)	(0.037)	(0.252)	(0.305)	(0.089)	(0.037)	(0.212)	(0.301)	(0.018)	(0.027)	(0.017)
1/1600	1600	−0.044	−0.017	−0.488	0.035	−0.347	−0.008	−0.496	0.025	−0.155	0.003	−0.001	0.007
		(0.331)	(0.072)	(0.026)	(0.149)	(0.297)	(0.062)	(0.026)	(0.132)	(0.308)	(0.017)	(0.020)	(0.015)

The table reports the bias (average deviation from the true value) and the standard deviation in parentheses for 1,000 draws. The true values for the midpoints of the continuous-time information share are (2/3, 1/3). The HIS is computed from a VECM(k) where k is successively increased with the sample size so that $k = \{1, 2, 4, 8, 16\}$. ρ_u and ρ_η denote the estimated innovation correlation for the discrete-time and continuous-time model, respectively.

Table C.15: Simulation results for the CAR(2) model in presence of i.i.d. microstructure noise ($\omega_1^2/\omega_2^2 = 0.0001/0.0005$, infill asymptotics)

		$N = 1$		
h	T	$\alpha_{h,\perp,1}$	HIS_1	IS_1^c
1/100	100	0.032	−0.073	0.019
		(0.441)	(0.334)	(0.159)
1/200	200	0.028	−0.092	0.029
		(0.443)	(0.339)	(0.123)
1/400	400	0.020	−0.134	0.026
		(0.451)	(0.366)	(0.107)
1/800	800	0.005	−0.159	0.031
		(0.458)	(0.304)	(0.083)
1/1600	1600	0.003	−0.187	−0.010
		(0.461)	(0.299)	(0.056)

The table reports the bias (average deviation from the true value) and the standard deviation in parentheses for 1,000 draws. All values are reported for the first market. The standard deviations for the second market are identical and the bias is identical up to a sign switch. The true values for the continuous time information share are (0.5, 0.5). The CS and HIS are computed from a VECM(k) where k is successively increased with the sample size so that $k = \{1, 2, 4, 8, 16\}$. The IS^c is based on an unconstrained likelihood.

Table C.16: Simulation results for the CAR(3) model

	$N = 100$				$N = 200$			
h	T	$\alpha_{h,\perp,1}$	HIS_1	IS_1^c	T	$\alpha_{h,\perp,1}$	HIS_1	IS_1^c
1	100	0.034	−0.010	−0.038	200	0.023	0.002	−0.023
		(0.141)	(0.173)	(0.152)		(0.093)	(0.122)	(0.100)
1/2	200	−0.016	−0.040	−0.035	400	−0.011	−0.025	−0.007
		(0.074)	(0.111)	(0.136)		(0.053)	(0.078)	(0.094)
1/4	400	−0.021	−0.055	−0.037	800	−0.018	−0.050	−0.011
		(0.025)	(0.044)	(0.133)		(0.016)	(0.029)	(0.091)
1/8	800	0.004	0.002	−0.027	1600	0.001	0.001	−0.007
		(0.024)	(0.038)	(0.122)		(0.013)	(0.023)	(0.084)
1/16	1600	0.046	0.035	−0.009	3200	0.020	0.022	−0.001
		(0.099)	(0.105)	(0.096)		(0.046)	(0.063)	(0.065)

The table reports the bias (average deviation from the true value) and the standard deviation in parentheses for 1,000 draws. All values are reported for the first market. The standard deviations for the second market are identical and the bias is identical up to a sign switch. The true values for the continuous-time information share are (0.8, 0.2). The CS and HIS are computed from a VECM(2).

Table C.17: Simulation results for the CAR(2) model in the presence of MA(1) microstructure noise ($\omega^2 = 0.001$)

	$N = 100$				$N = 200$			
h	T	$\alpha_{h,\perp,1}$	HIS_1	IS_1^c	T	$\alpha_{h,\perp,1}$	HIS_1	IS_1^c
1	100	0.002	−0.064	−0.032	200	0.001	−0.056	−0.004
		(0.119)	(0.133)	(0.148)		(0.082)	(0.093)	(0.103)
1/2	200	−0.008	−0.038	−0.013	400	−0.018	−0.046	−0.018
		(0.082)	(0.111)	(0.115)		(0.059)	(0.084)	(0.086)
1/4	400	−0.001	−0.023	−0.025	800	0.006	−0.005	−0.005
		(0.083)	(0.114)	(0.117)		(0.057)	(0.077)	(0.080)
1/8	800	0.125	0.090	−0.008	1600	0.115	0.103	−0.006
		(0.134)	(0.116)	(0.109)		(0.092)	(0.082)	(0.078)
1/16	1600	0.297	0.132	−0.013	3200	0.299	0.166	−0.006
		(0.224)	(0.117)	(0.102)		(0.157)	(0.061)	(0.067)

The table reports the bias (average deviation from the true value) and the standard deviation in parentheses for 1,000 draws. All values are reported for the first market. The standard deviations for the second market are identical and the bias is identical up to a sign switch. The true values for the continuous-time information share are (0.8, 0.2). The CS and HIS are computed from a VECM(1). The MSN dynamics are governed by the coefficient matrix $\Theta = diag(0.25, 0.25)$.

Table C.18: Simulation results for the CAR(2) model in the presence of endogenous MA(1) microstructure noise ($\omega^2 = 0.001$)

		$N = 100$				$N = 200$		
h	T	$\alpha_{h,\perp,1}$	HIS_1	IS_1^c	T	$\alpha_{h,\perp,1}$	HIS_1	IS_1^c
1	100	−0.011	−0.082	−0.007	200	−0.014	−0.066	−0.004
		(0.121)	(0.131)	(0.046)		(0.086)	(0.104)	(0.040)
1/2	200	−0.022	−0.049	−0.025	400	−0.037	−0.064	−0.035
		(0.080)	(0.115)	(0.126)		(0.053)	(0.083)	(0.088)
1/4	400	−0.011	−0.021	−0.010	800	−0.018	−0.027	−0.008
		(0.082)	(0.113)	(0.102)		(0.055)	(0.083)	(0.076)
1/8	800	0.089	0.076	0.001	1600	0.095	0.095	−0.001
		(0.120)	(0.128)	(0.036)		(0.093)	(0.089)	(0.013)
1/16	1600	0.306	0.137	−0.001	3200	0.311	0.170	−0.001
		(0.223)	(0.124)	(0.001)		(0.154)	(0.061)	(0.007)

The table reports the bias (average deviation from the true value) and the standard deviation in parentheses for 1,000 draws. All values are reported for the first market. The standard deviations for the second market are identical and the bias is identical up to a sign switch. The true values for the continuous-time information share are (0.8, 0.2). The CS and HIS are computed from a VECM(1). The MSN dynamics are governed by the coefficient matrix $\Theta = diag(0.25, 0.25)$.

D Additional empirical results

D.1 Preliminary analyses

Figure D.1: Volatility signature plots (IBM)
The figure depicts the volatility of the NYSE and NASDAQ returns. The x-axis is log-scaled.

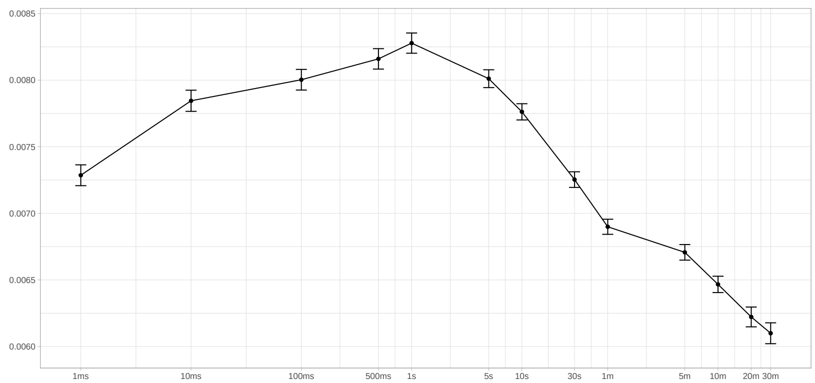

(a) NYSE

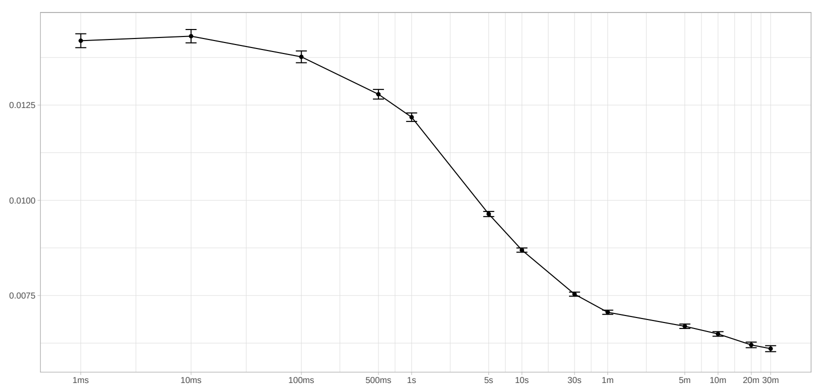

(b) NASDAQ

Figure D.2: Volatility signature plots (NVDA)
The figure depicts the volatility of the NYSE and NASDAQ returns. The x-axis is log-scaled.

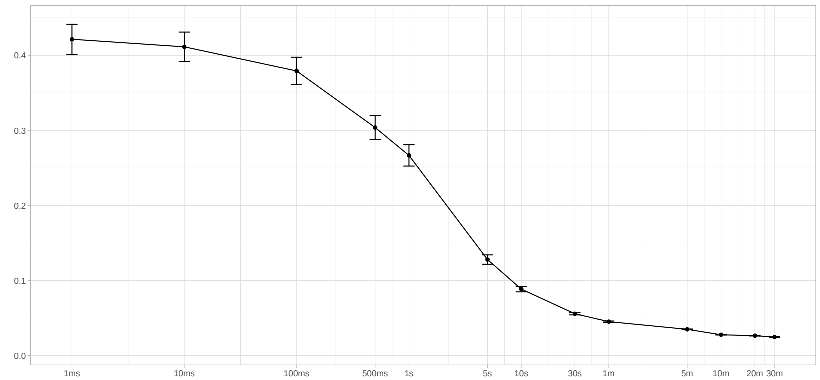

(a) NYSE

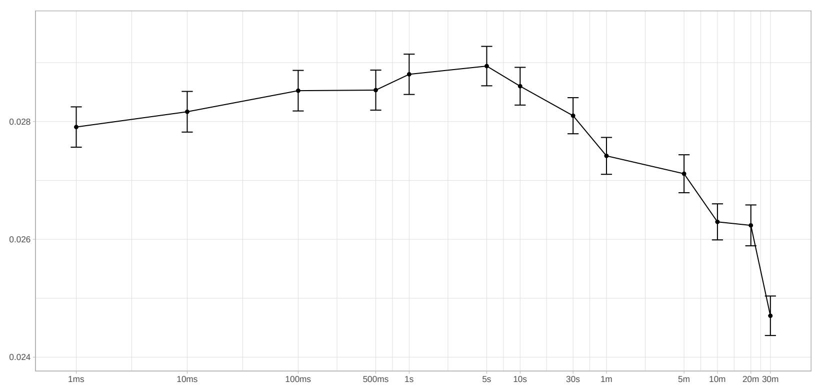

(b) NASDAQ

Table D.1: Percentage of sampling intervals without price changes.

	1ms	10ms	100ms	500ms	1s	5s	10s	30s	1m	5m	10m	20m	30m
							IBM						
NYSE	0.999	0.996	0.964	0.848	0.738	0.332	0.174	0.058	0.038	0.019	0.014	0.011	0.008
NASDAQ	0.999	0.995	0.961	0.840	0.727	0.324	0.169	0.056	0.037	0.017	0.011	0.009	0.004
							NVDA						
NYSE	0.999	0.996	0.963	0.854	0.751	0.388	0.217	0.053	0.016	0.002	0.000	0.000	0.000
NASDAQ	0.999	0.996	0.964	0.855	0.750	0.352	0.171	0.026	0.006	0.001	0.001	0.002	0.000

D.2 Diagonality tests

Figure D.3: CAR(2) results (IBM), p-values for the diagonality hypothesis

This figure depicts the p-values corresponding to the diagonality hypothesis for all trading days from January to March 2021. The horizontal dashed line indicates the 5% significance level. The p-values below the Bonferroni-corrected significance level are colored blue while those above are colored black.

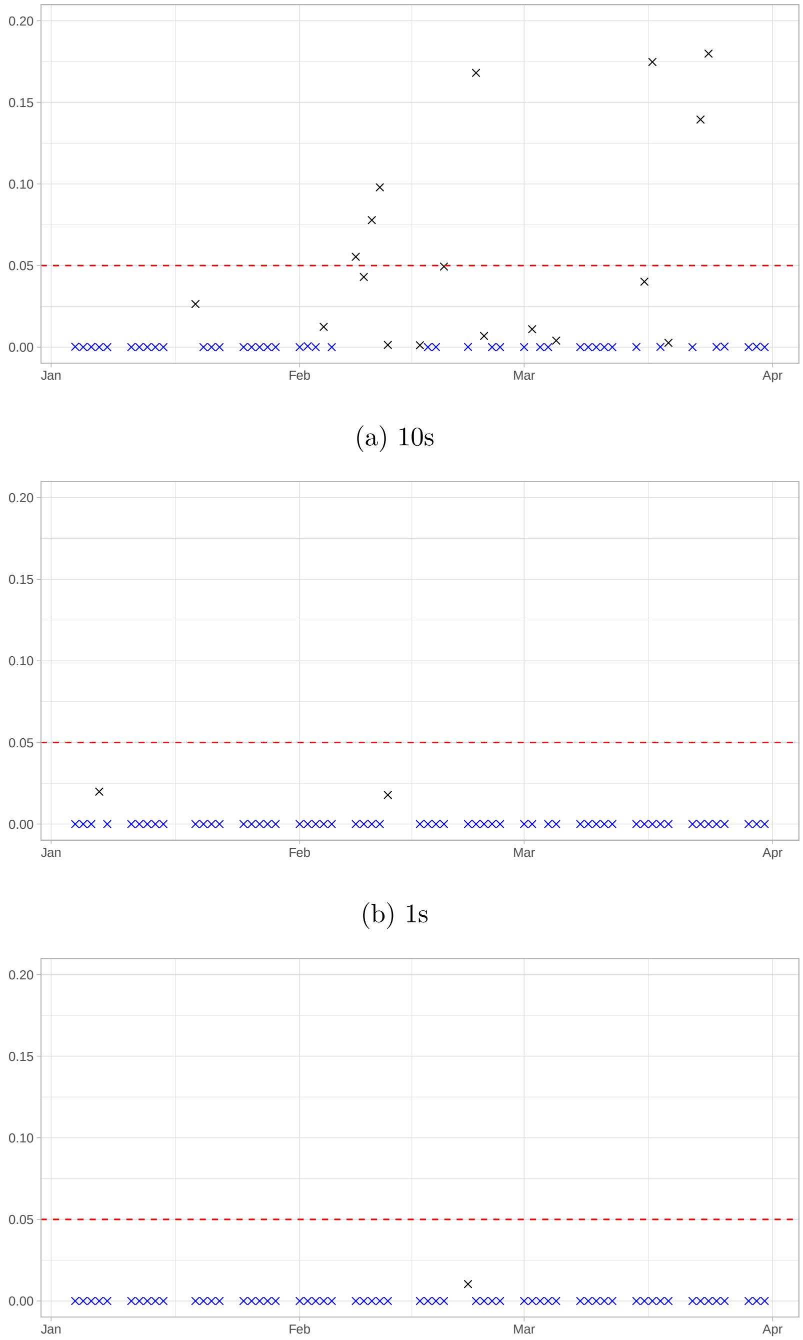

(a) 10s

(b) 1s

(c) 100ms

Figure D.4: CAR(2) results (NVDA), p-values for the diagonality hypothesis

This figure depicts the p-values corresponding to the diagonality hypothesis for all trading days from January to March 2021. The horizontal dashed line indicates the 5% significance level. The p-values below the Bonferroni-corrected significance level are colored blue while those above are colored black.

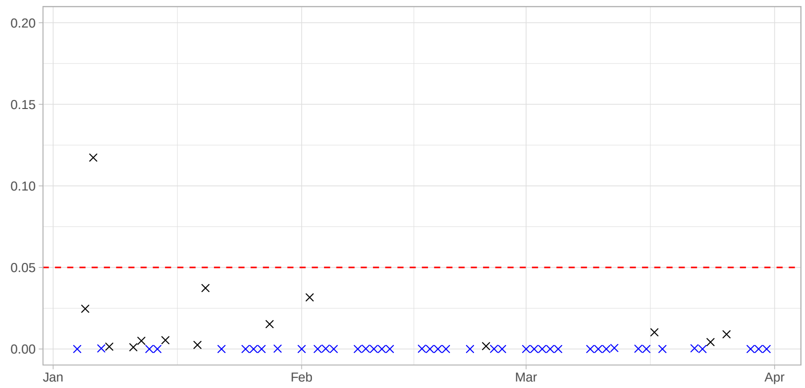

(a) 10s

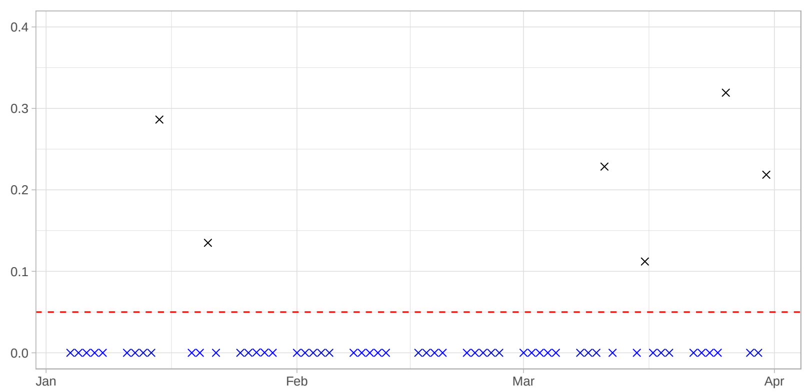

(b) 1s

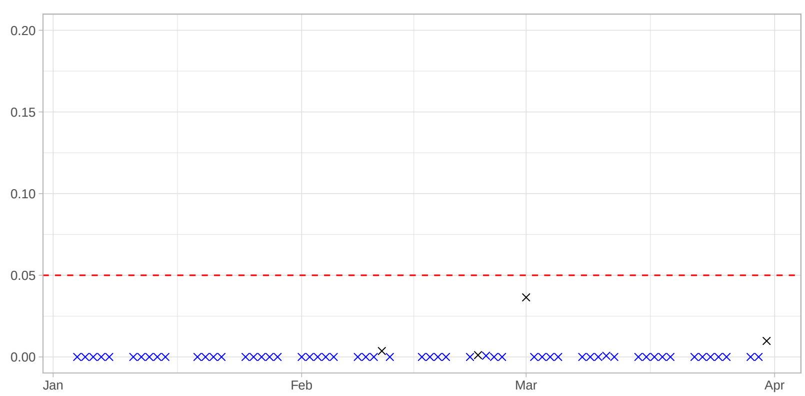

(c) 100ms

D.3 Robustness checks – exact discretization

Figure D.5: CAR(2) results (IBM), not refreshed, constrained
This figure depicts the daily continuous time information share of the NYSE estimated at different sampling frequency. The results are obtained from the constrained likelihood forcing the covariance matrix to be diagonal. The red dashed line indicates the average information share over all trading days (Jan – Mar 2021).

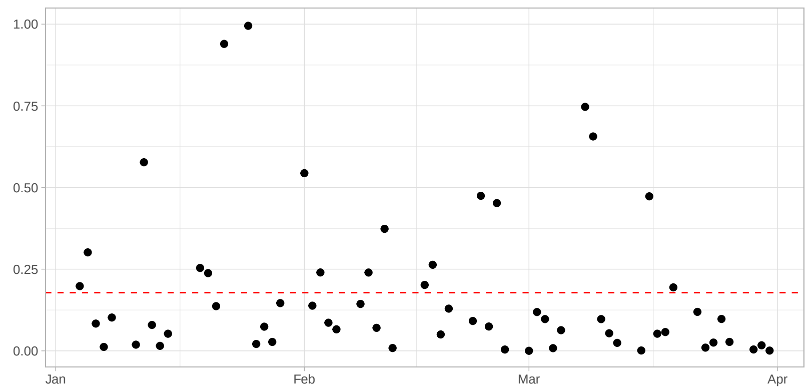

(a) 10s

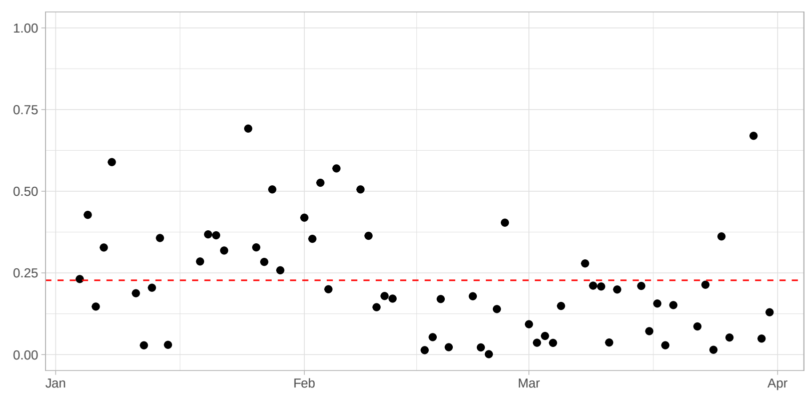

(b) 1s

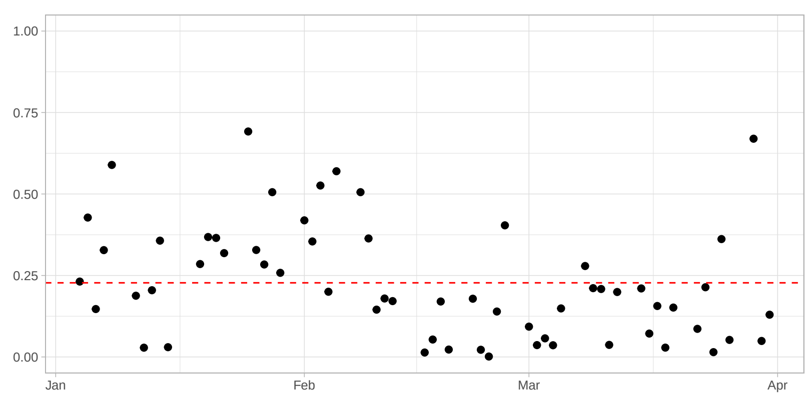

(c) 100ms

Figure D.6: High-resolution VECM results (IBM), not refreshed
This figure depicts the daily HIS of the NYSE estimated at different sampling frequencies during the period from January to March 2021. The vertical bars indicate the daily spread between lower and upper bound. The red dashed line indicates the average HIS over all trading days. The red shade indicates the average spread between lower and upper bound of the HIS.

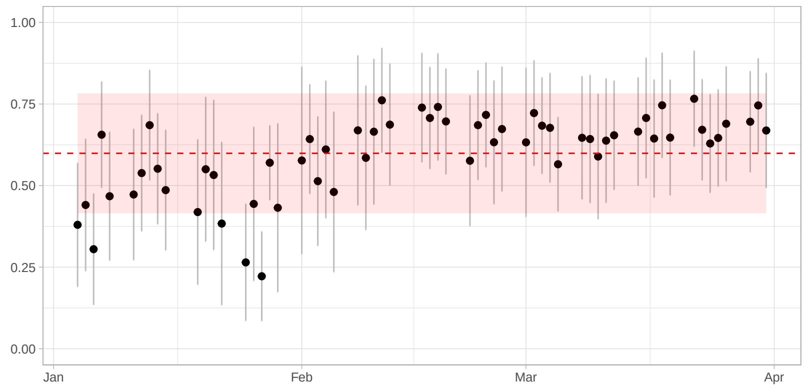

(a) 100ms

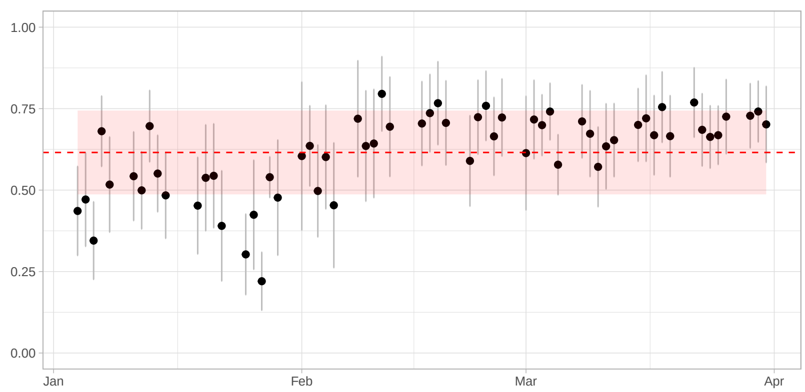

(b) 10ms

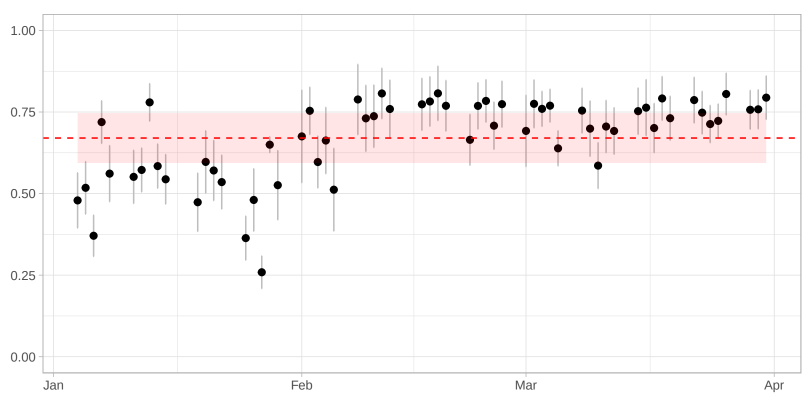

(c) 1ms

Figure D.7: CAR(2) results (IBM), refresh time, constrained
This figure depicts the daily continuous time information share of the primary listing exchange (NYSE) estimated at different sampling frequency. The red dashed line indicates the average information share over all trading days (Jan – Mar 2021).

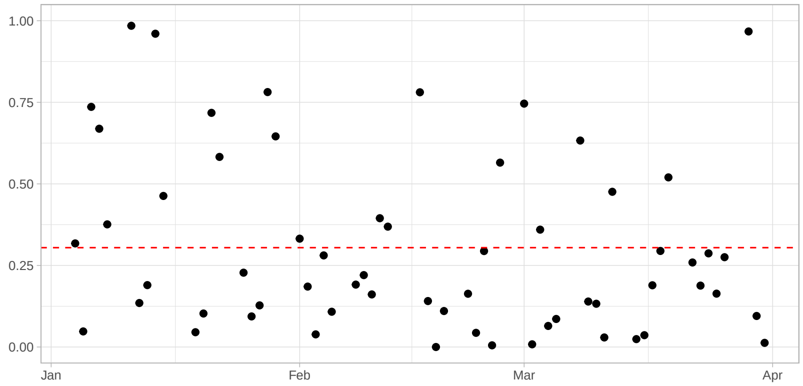

(a) 10s

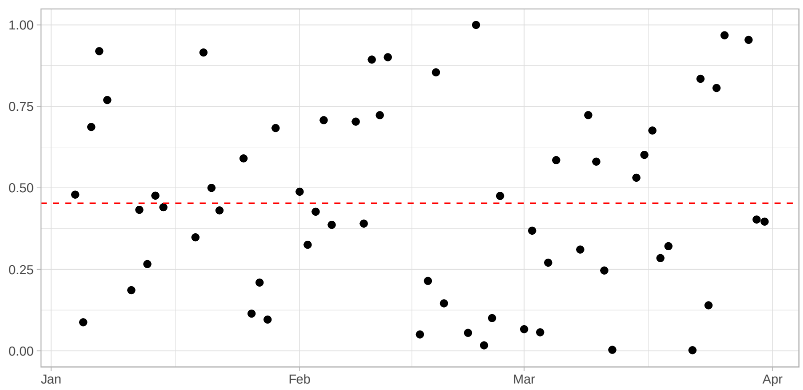

(b) 1s

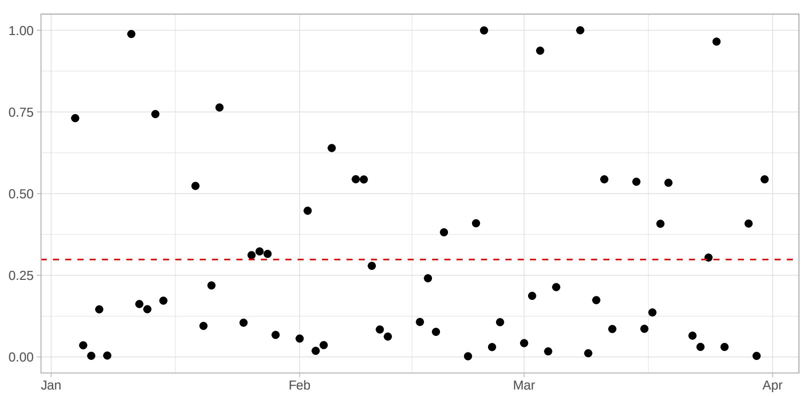

(c) 100ms

D.4 Robustness checks – Kalman filter approach

Table D.2: Summary of empirical results: Kalman filter approach with MA(1) errors

						common news factor:						
	HIS_N	$\bar{\Theta}_N$	$\bar{\Theta}_{T,OQ}$	$\tilde{\omega}^2_N$	$\tilde{\omega}^2_{T,OQ}$	MIS_N	$\text{MIS}_{T,OQ}$	CIS	$\bar{\Theta}_N$	$\bar{\Theta}_{T,OQ}$	$\tilde{\omega}^2_N$	$\tilde{\omega}^2_{T,OQ}$
					IBM							
10s	0.493	0.125	0.090	0.206	0.223	0.026	0.004	0.971	0.232	0.232	0.215	0.239
1s	0.478	0.137	0.133	0.351	0.549	0.063	0.068	0.869	0.241	0.256	0.362	0.609
100ms	0.468	0.134	0.139	0.593	0.963	0.107	0.230	0.663	0.242	0.250	0.641	1.034
ticks	0.495	0.288	0.196	1.939	6.700	0.043	0.048	0.909	0.532	0.392	1.911	6.367
					NVDA							
10s	0.493	0.226	0.208	2.953	0.660	0.036	0.032	0.931	0.253	0.252	1.801	0.736
1s	0.395	0.251	0.191	9.580	1.201	0.238	0.181	0.581	0.179	0.188	15.499	0.832
100ms	0.522	0.322	0.296	22.053	2.297	0.530	0.154	0.318	0.309	0.324	21.469	2.252
ticks	0.543	0.496	0.413	75.924	6.880	0.218	0.136	0.645	0.489	0.415	73.974	6.864

The table reports the HIS midpoints for the NYSE (HIS_N) and the rescaled noise variances for both markets ($\times 10^{-4}$). $\bar{\Theta}_N$ and $\bar{\Theta}_{T,OQ}$ denote the average autoregressive coefficient of the noise process. To compare the noise levels across frequencies, we denote the sum of squares by $\tilde{\omega}^2_N$ and $\tilde{\omega}^2_{T,OQ}$. MIS_N and $\text{MIS}_{T,OQ}$ are the market-specific information shares and CIS is the common information share attributed to the common news factor. The noise levels are computed for the likelihood function with and without common news factor structure.

Figure D.8: CAR(2) results (IBM), refresh time, Kalman filter (i.i.d. errors)
This figure depicts the daily continuous-time information share of the primary listing exchange (NYSE) estimated at different sampling frequencies. The vertical bars indicate the daily spread between lower and upper bound. The red dashed line indicates the average information share over all trading days (Jan – Mar 2021). The red shade indicates the average spread between lower and upper bound of the information share.

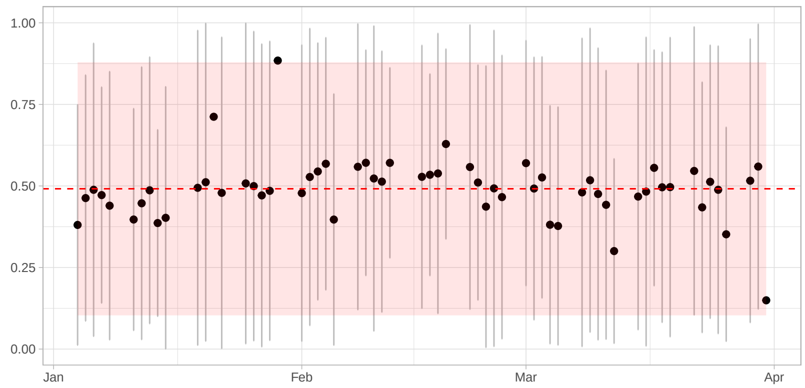

(a) 10s

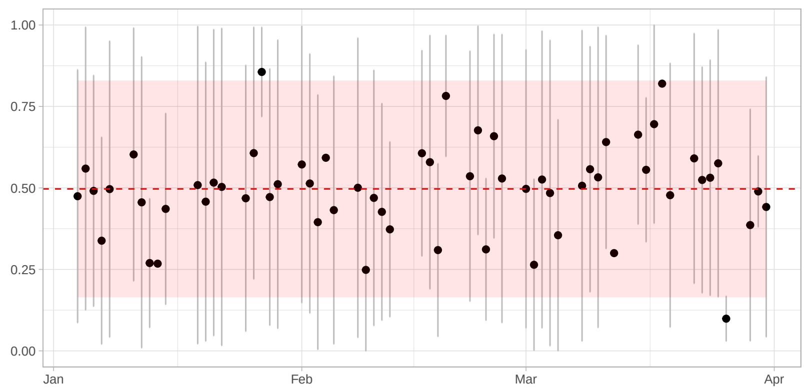

(b) 1s

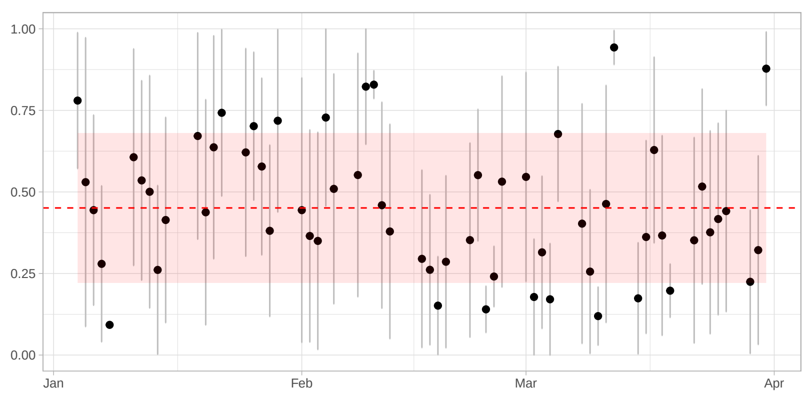

(c) 100ms

Figure D.9: CAR(2) results (NVDA), refresh time, Kalman filter (i.i.d. errors)
This figure depicts the daily continuous-time information share of the primary listing exchange (NASDAQ) estimated at different sampling frequencies. The vertical bars indicate the daily spread between lower and upper bound. The red dashed line indicates the average information share over all trading days (Jan – Mar 2021). The red shade indicates the average spread between lower and upper bound of the information share.

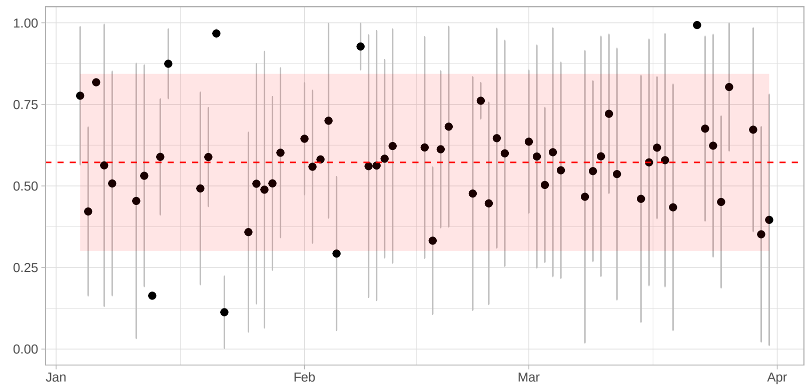

(a) 10s

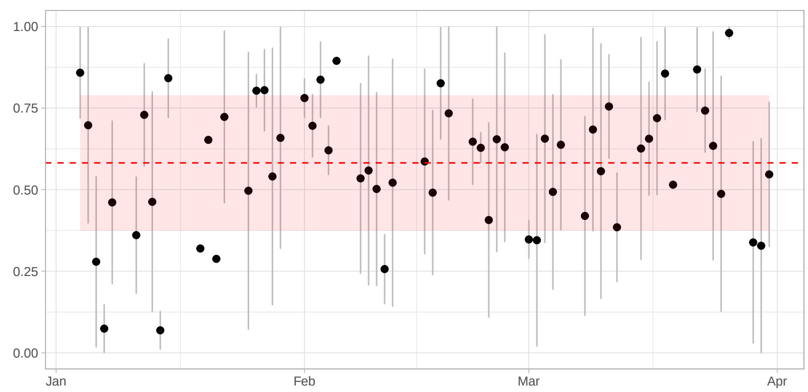

(b) 1s

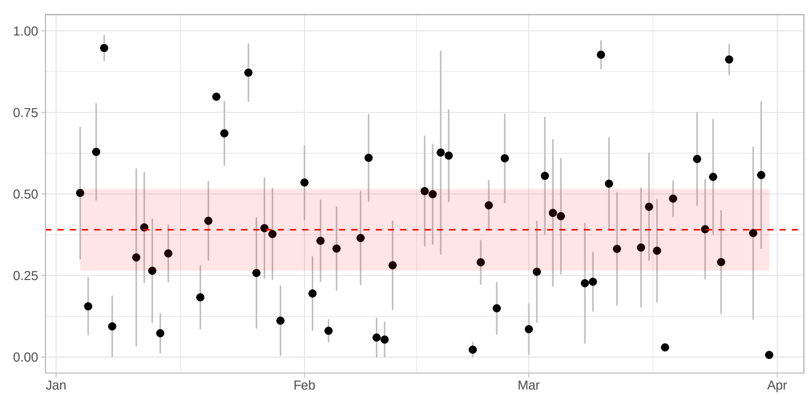

(c) 100ms

Figure D.10: CAR(2) results, refresh time, Kalman filter (i.i.d. errors)

This figure depicts the daily market-specific continuous-time information shares of the NYSE in black and the NASDAQ in grey estimated at tick time. The continuous-time common information share is depicted in blue.

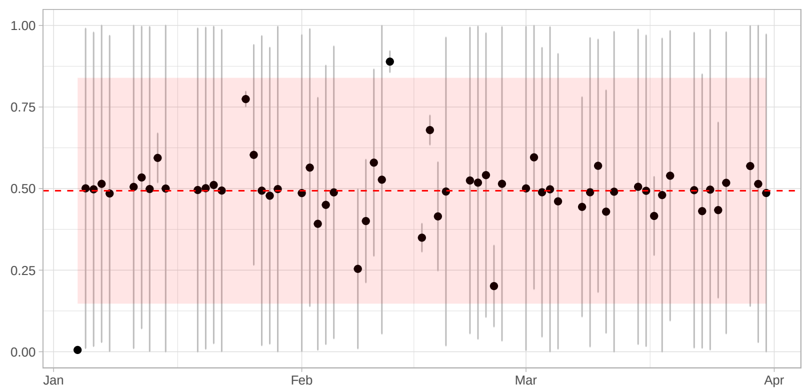

(a) IBM

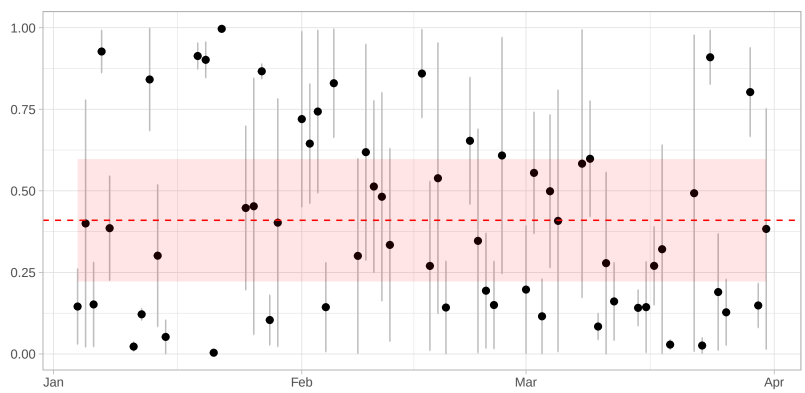

(b) NVDA

Figure D.11: CAR(2) results (IBM), refresh time, Kalman filter (i.i.d. errors), common factor error

This figure depicts the daily market-specific continuous-time information shares of the primary listing exchange (NYSE) in black and the NASDAQ in grey estimated at different sampling frequencies. The continuous-time common information share is depicted in blue.

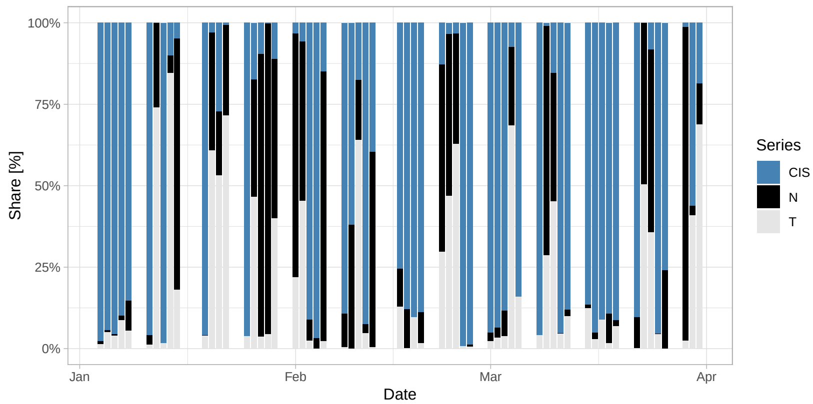

(a) 10s

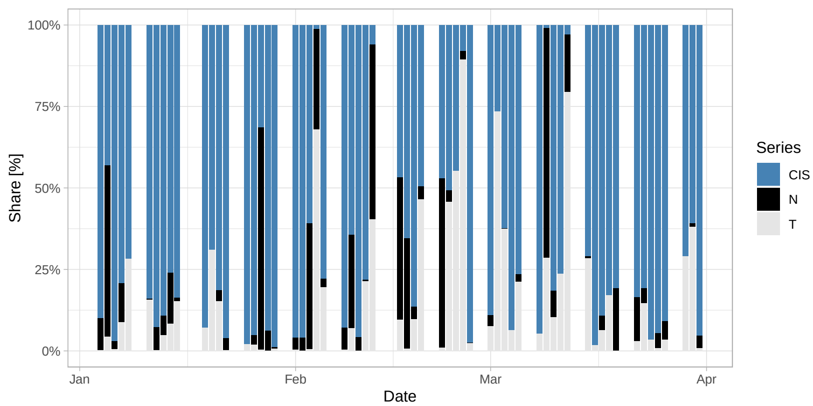

(b) 1s

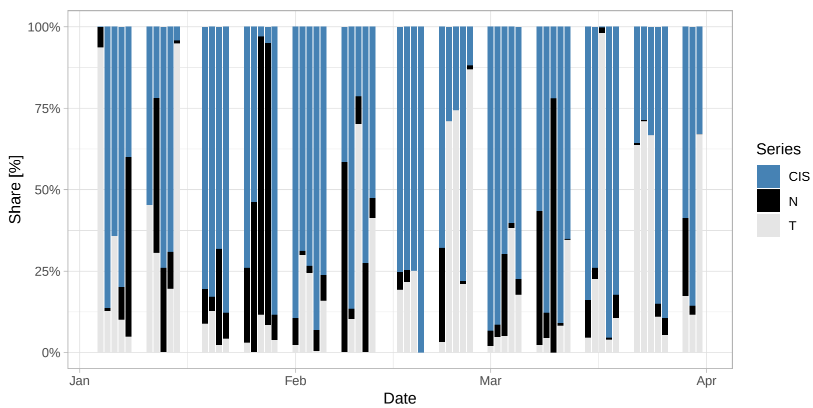

(c) 100ms

Figure D.12: CAR(2) results (NVDA), refresh time, Kalman filter (i.i.d. errors), common factor error

This figure depicts the daily market-specific continuous-time information shares of the primary listing exchange (NASDAQ) in grey and the NYSE in black estimated at different sampling frequencies. The continuous-time common information share is depicted in blue.

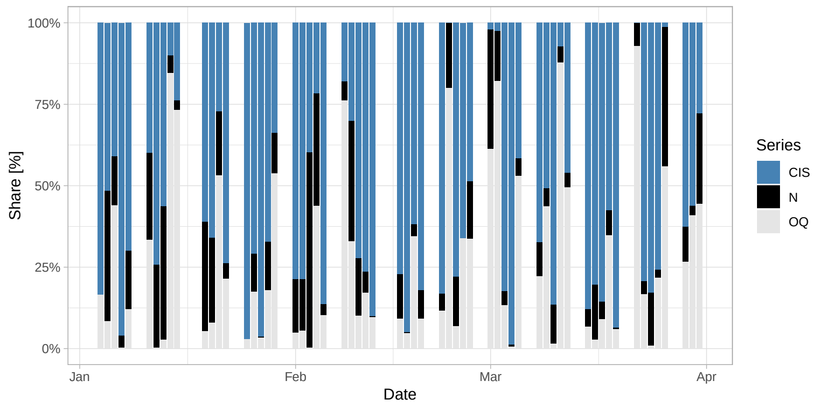

(a) 10s

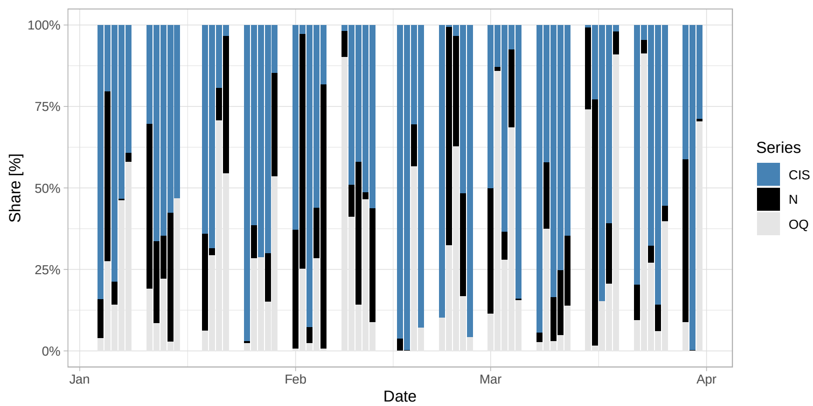

(b) 1s

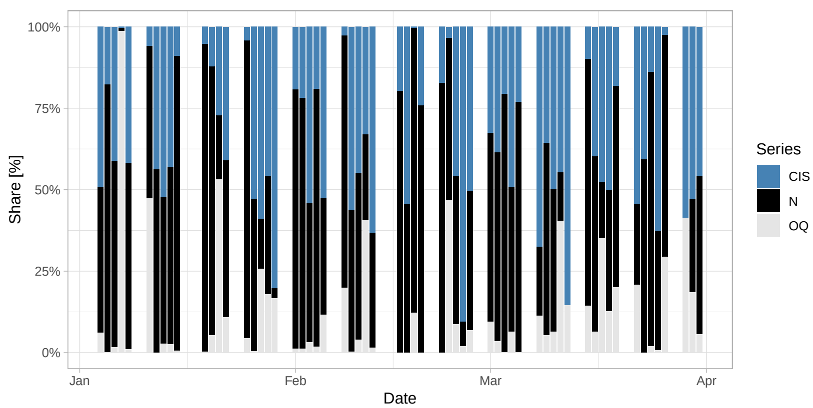

(c) 100ms

Figure D.13: CAR(2) results (IBM), refresh time, Kalman filter (MA(1) errors)
This figure depicts the daily continuous-time information share of the primary listing exchange (NYSE) estimated at different sampling frequencies. The vertical bars indicate the daily spread between lower and upper bound. The red dashed line indicates the average information share over all trading days (Jan – Mar 2021). The red shade indicates the average spread between lower and upper bound of the information share.

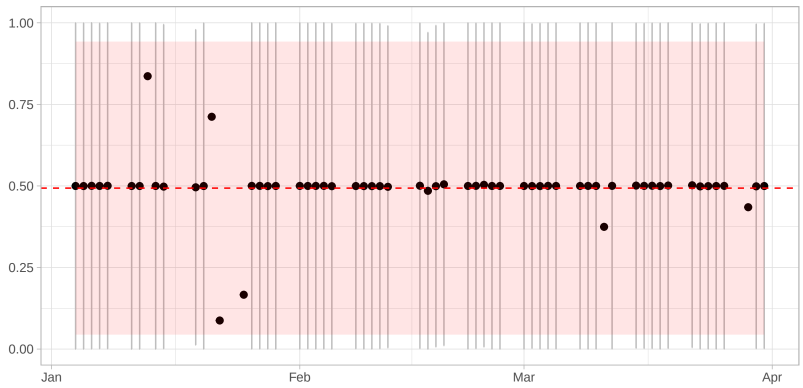

(a) 10s

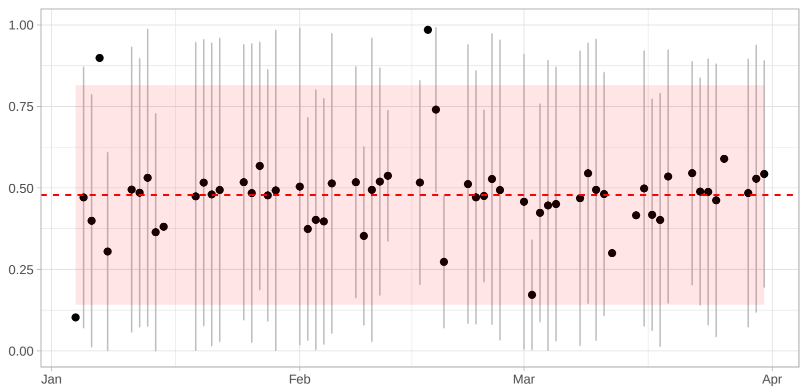

(b) 1s

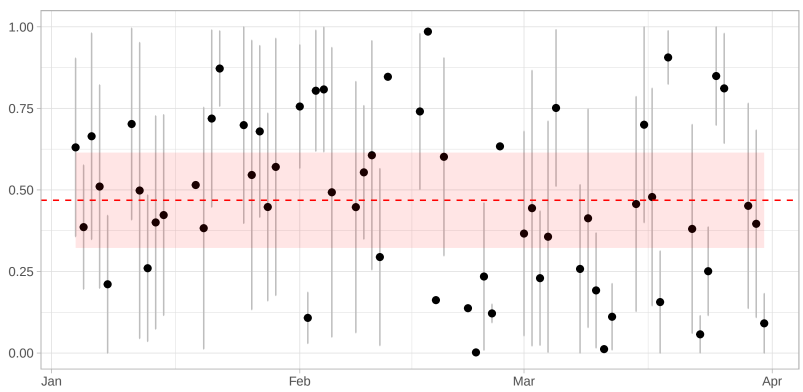

(c) 100ms

Figure D.14: CAR(2) results (NVDA), refresh time, Kalman filter (MA(1) errors)
This figure depicts the daily continuous-time information share of the primary listing exchange (NASDAQ) estimated at different sampling frequencies. The vertical bars indicate the daily spread between lower and upper bound. The red dashed line indicates the average information share over all trading days (Jan – Mar 2021). The red shade indicates the average spread between lower and upper bound of the information share.

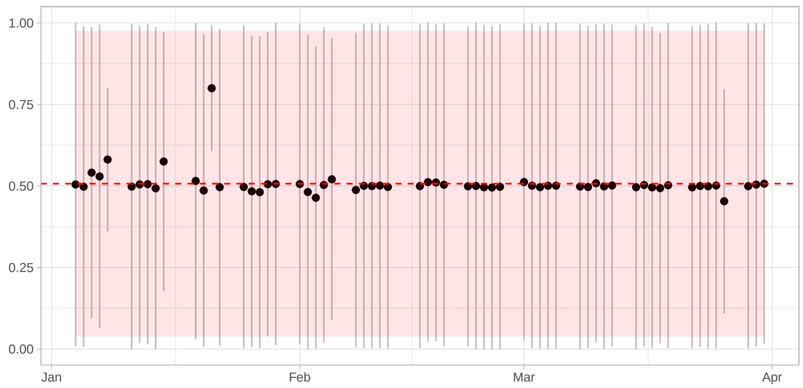

(a) 10s

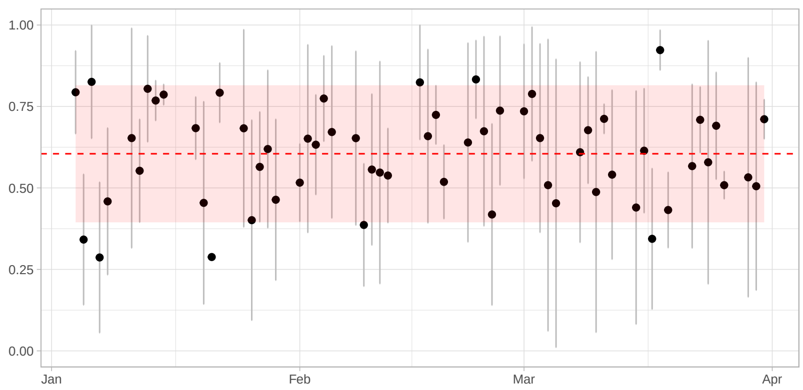

(b) 1s

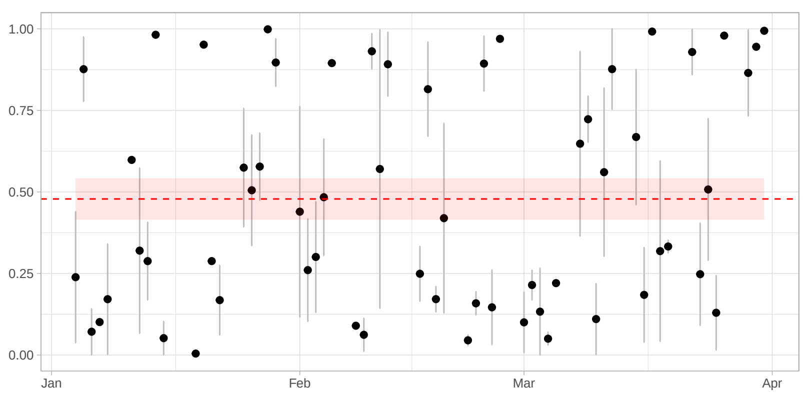

(c) 100ms

Figure D.15: CAR(2) results, refresh time, Kalman filter (MA(1) errors)
This figure depicts the daily market-specific continuous-time information shares of the NYSE in black and the NASDAQ in grey estimated at tick time. The continuous-time common information share is depicted in blue.

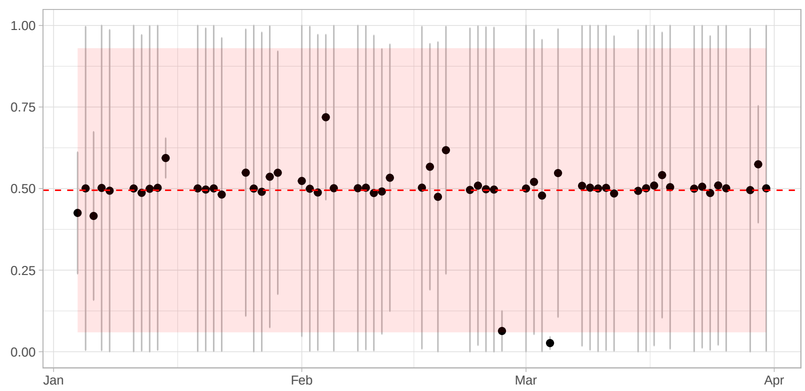

(a) IBM

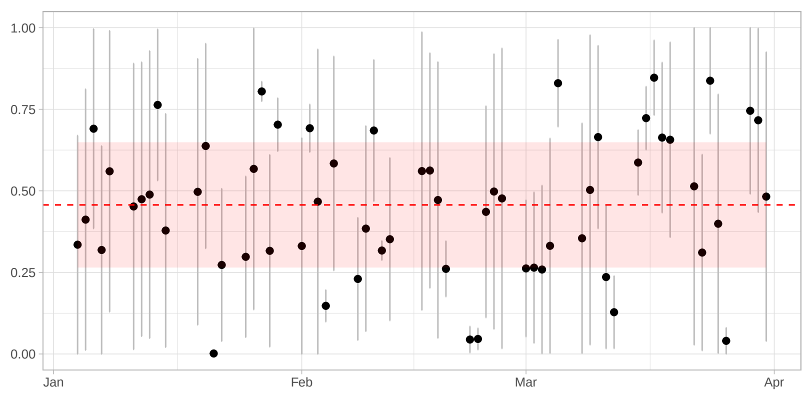

(b) NVDA

Figure D.16: CAR(2) results (IBM), refresh time, Kalman filter (MA(1) errors), common factor error

This figure depicts the daily market-specific continuous-time information shares of the primary listing exchange (NYSE) in black and the NASDAQ in grey estimated at different sampling frequencies. The continuous-time common information share is depicted in blue.

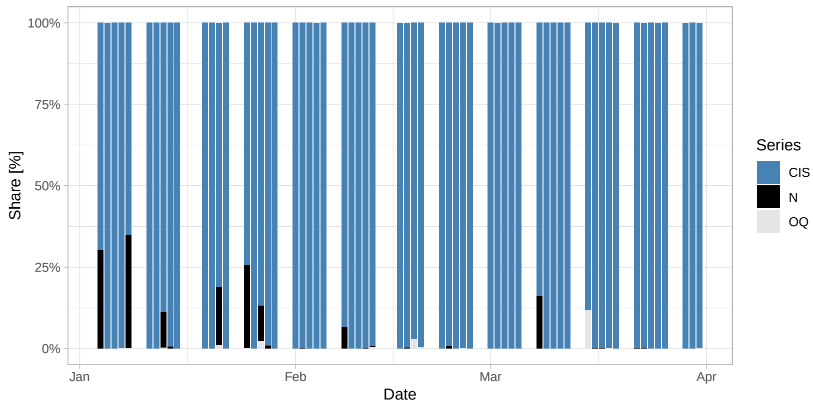

(a) 10s

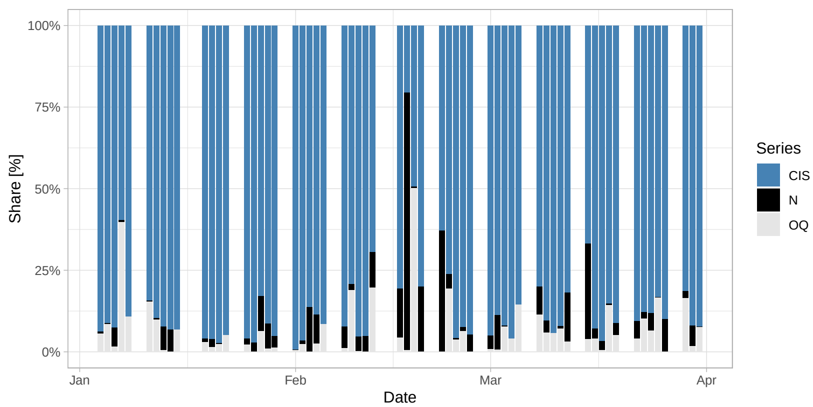

(b) 1s

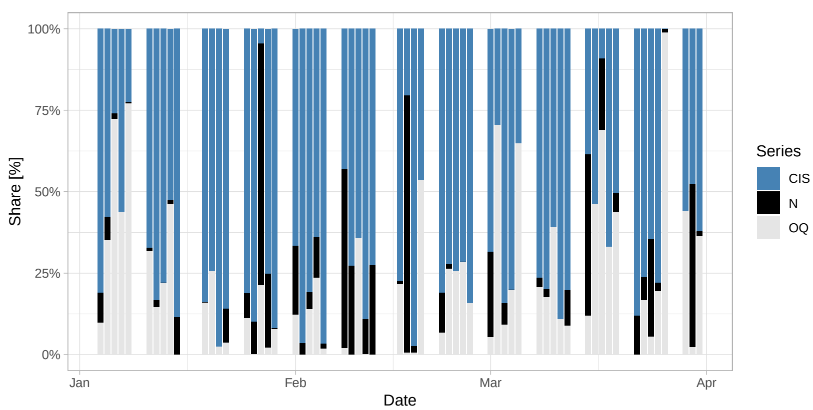

(c) 100ms

Figure D.17: CAR(2) results (NVDA), refresh time, Kalman filter (MA(1) errors), common factor error

This figure depicts the daily market-specific continuous-time information shares of the primary listing exchange (NASDAQ) in grey and the NYSE in black estimated at different sampling frequencies. The continuous-time common information share is depicted in blue.

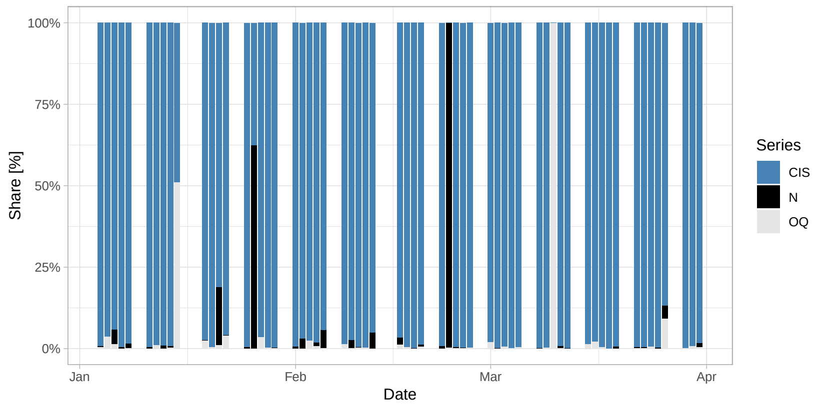

(a) 10s

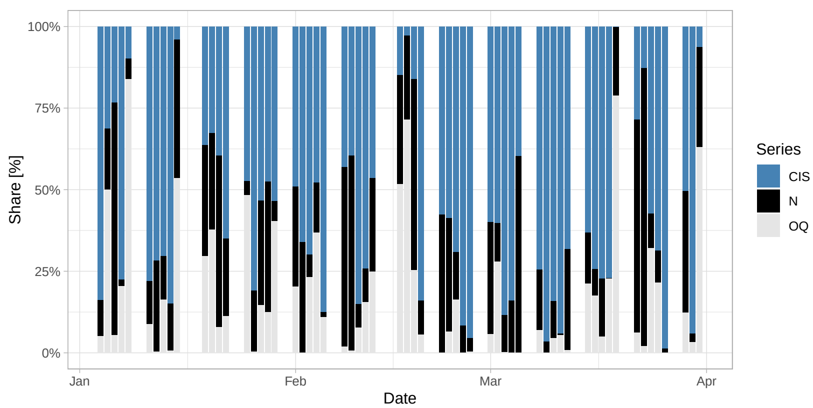

(b) 1s

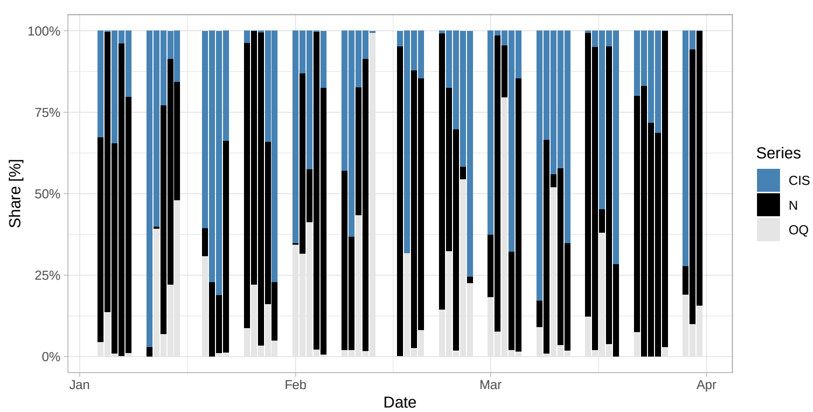

(c) 100ms

Figure D.18: CAR(2) results, common factor error, Kalman filter (MA(1) errors)
This figure depicts the daily market-specific continuous-time information shares of the NYSE in black and the NASDAQ in grey estimated at tick time. The continuous-time common information share is depicted in blue. The median duration between ticks is 5ms (IBM) and 74ms (NVDA).

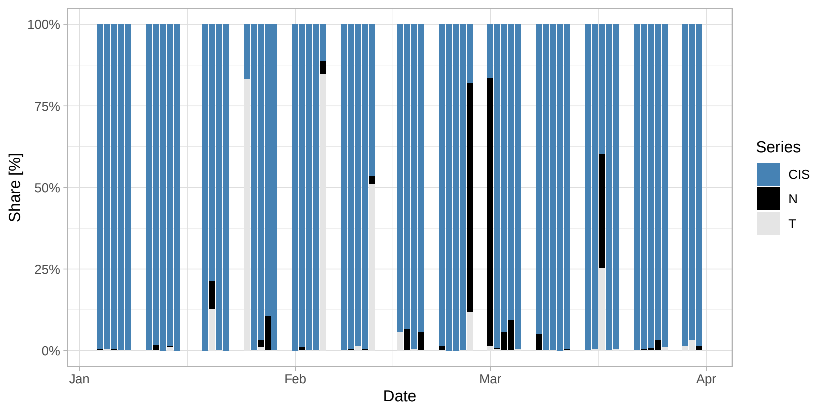

(a) IBM

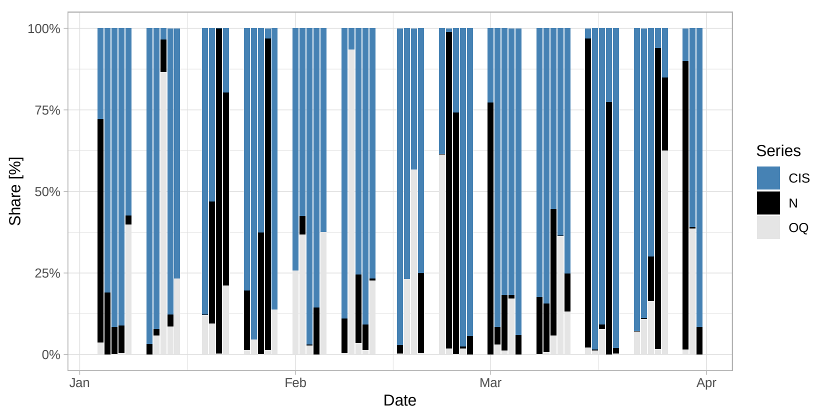

(b) NVDA

Figure D.19: CAR(3) results, common factor error, Kalman filter (i.i.d. errors)
This figure depicts the daily market-specific continuous-time information shares of the NYSE in black and the NASDAQ in grey estimated at tick time. The continuous-time common information share is depicted in blue. The median duration between ticks is 5ms (IBM) and 74ms (NVDA).

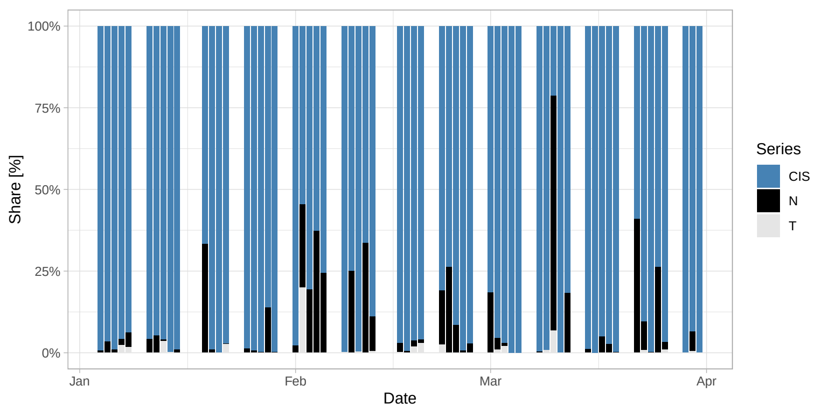

(a) IBM

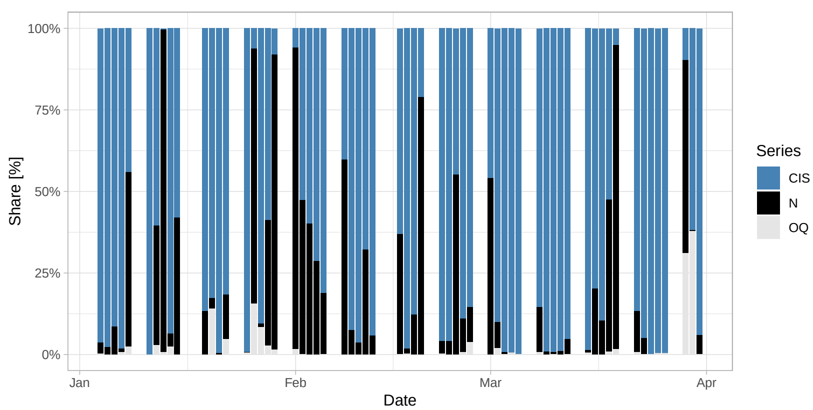

(b) NVDA

References

Amemiya, T., 1985. Advanced Econometrics. Harvard University Press.

Chambers, M.J., 1999. Discrete time representation of stationary and non-stationary continuous time systems. Journal of Economic Dynamics and Control 23, 619–639. doi:10.1016/s0165-1889(98)00032-3.

Comte, F., 1999. Discrete and continuous time cointegration. Journal of Econometrics 88, 207–226. doi:10.1016/S0304-4076(98)00025-6.

Hasbrouck, J., 2021. Price Discovery in High Resolution. Journal of Financial Econometrics 19, 395–430. doi:10.1093/jjfinec/nbz027.

Newey, W.K., McFadden, D., 1994. Chapter 36: Large sample estimation and hypothesis testing, in: Engle, R., McFadden, D. (Eds.), Handbook of Econometrics, Vol.4, pp. 2111–2245.

Van Loan, C.F., 1978. Computing Integrals Involving the Matrix Exponential. IEEE Transactions on Automatic Control 23, 395–404. doi:10.1109/TAC.1978.1101743.

Vlaar, P.J.G., 2004. On the asymptotic distribution of impulse response functions with long-run restrictions. Econometric Theory 20, 891–903. doi:10.1017/S0266466604205047.